An analytic model for Tropical cyclone outer winds

Timothy Wallace Cronin[1]

[1]MIT

April 4, 2023

Abstract

The variation of Tropical cyclone azimuthal wind speed (V) with distance from storm center (r) is a fundamental aspect of storm structure that has important implications for risk and damages. The theoretical model of Emanuel (2004), which applies well outside the rainy core of the storm, matches radiatively-driven subsidence and Ekman suction rates at the top of the boundary layer to obtain a nonlinear differential equation for dV/dr. This model is particularly appealing because of its strong physical foundation, but has no known analytic solution for V(r). In this paper, I obtain an analytic solution to V(r) for the Emanuel (2004) outer wind model. Following previous work, I then use this solution to explore properties of merged wind models that combine the outer model with an inner model that applies to the rainy core of a storm.

An analytic model for Tropical cyclone outer winds

Timothy W. Cronin[1]

[1]Program in Atmospheres, Ocean, and Climate, MIT, Cambridge, Massachusetts, USA

Key Points:

- Analytic solutions are derived for the previously unsolved outer wind model of Emanuel (2004).
- Analytic wind profile calculations enable faster merged wind profile calculations, following Chavas et al. (2015).
- Scaling of merged wind profiles suggests decreases in the radius of maximum wind with warming, at constant outer size.

Corresponding author: Timothy Cronin, `twcronin@mit.edu`

Abstract

The variation of Tropical cyclone azimuthal wind speed (V) with distance from storm center (r) is a fundamental aspect of storm structure that has important implications for risk and damages. The theoretical model of Emanuel (2004), which applies well outside the rainy core of the storm, matches radiatively-driven subsidence and Ekman suction rates at the top of the boundary layer to obtain a nonlinear differential equation for dV/dr. This model is particularly appealing because of its strong physical foundation, but has no known analytic solution for $V(r)$. In this paper, I obtain an analytic solution to $V(r)$ for the Emanuel (2004) outer wind model. Following previous work, I then use this solution to explore properties of merged wind models that combine the outer model with an inner model that applies to the rainy core of a storm.

Plain Language Summary

The swirling winds of hurricanes extend far away from their centers, fading away into background weather. Previous work has proposed a theoretical model to explain how these swirling winds decrease with distance from the storm center for areas outside the rainy core of the storm. But this model has not previously been solved with pencil-and-paper methods. I find a new mathematical formula that solves the model for how winds weaken away from the center of a hurricane. I then use the solutions to examine how hurricane winds near the center of a storm relate to the winds far from the center, and what this implies about how hurricanes behave.

1 Introduction

The swirling or azimuthal winds (V) of a Tropical cyclone increase rapidly away from its calm eye to a maximum in the eyewall, then decrease much more gradually with radius (r), fading away into the background flow. This radial profile of swirling winds – which I will refer to as the “wind structure,” “wind profile,” or simply $V(r)$ – encapsulates important relationships among variables in a Tropical cyclone, including the maximum swirling wind speed, V_m, the radius at which these maximum winds are attained, r_m, and the far outer radius of the storm where the winds vanish, r_0. These all can influence the destructive capability of a storm, with outer size of a storm particularly important for storm surge damage (e.g., Powell & Reinhold, 2007; Irish & Resio, 2010; Lin & Chavas, 2012). For real storms, r_0 is difficult to measure directly and requires azimuthal averaging in any nonzero background flow, so Tropical cyclone size is commonly quantified using the radius of a certain fixed value of wind speed (e.g., gale-force winds) or the radius of a closed surface pressure contour, instead of the radius of vanishing winds (e.g., Frank, 1977; Merrill, 1984; Chavas & Emanuel, 2010). Numerous empirical models of wind structure have been developed and are widely used; for example, the elegant work of Holland (1980) fits the observed dependence of pressure on radius using a logarithmic rectangular hyperbola, with gradient wind balance then enabling calculation of $V(r)$. Empirical wind structure models, however, cannot identify the dynamical or kinematic constraints that might bound or link intensity, radius of maximum winds, and outer size, or provide insight on how $V(r)$ might change in a warming climate. Emanuel (2004) and Emanuel and Rotunno (2011) developed physics-based models of, respectively, storm outer and inner structure: these two were cleverly merged into a complete theoretical wind model by Chavas et al. (2015) (See schematic of merged winds in Figure 1). The inner wind model of Emanuel and Rotunno (2011) assumes a slantwise-moist-neutral core of the storm, where the radial gradients in wind speed outside the eyewall are constrained by wind shear and mixing in the outflow, and has known analytic solutions (in the limit of a cyclostrophic vortex). The outer wind model of Emanuel (2004) is based on the (sound) assumption that subsidence due to radiative cooling matches Ekman suction at the top of the boundary layer in the outer region of the storm where there is little rain and deep convection. This outer wind model, however, has been formulated only as a nonlinear differential equation for dV/dr, and lacks a known analytic solution for $V(r)$.

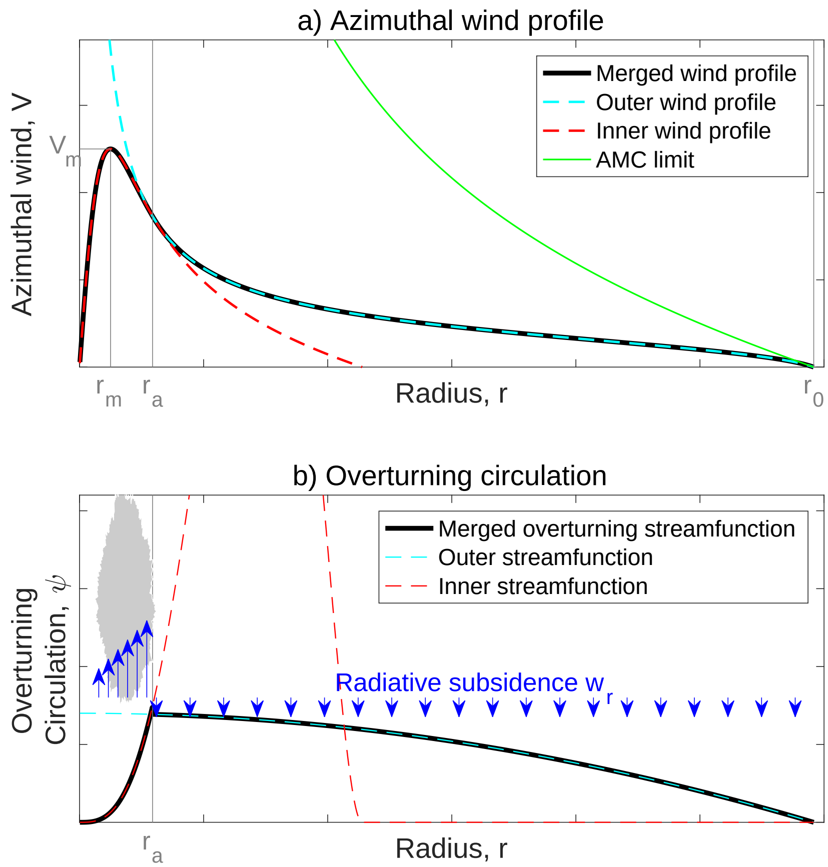

Figure 1. a) Azimuthal or swirling winds, V, of a Tropical cyclone plotted against radius, r. General features include the radius of maximum wind, r_m, the maximum wind speed V_m, and the radius of vanishing wind, r_0. The specific profile drawn in black merges the Emanuel (2004) outer wind model (cyan dashed line) and the Emanuel and Rotunno (2011) inner wind model (red dashed line), following Chavas et al. (2015). The theoretical angular-momentum-conserving wind profile (green), and the merge radius r_a are also drawn. b) The overturning circulation in the radius-height plane generally includes ascent at small radii, and sinking at large radii. Merged wind profiles of Chavas et al. (2015) have a continuous overturning streamfunction (ψ) at r_a, but a discontinuity in vertical velocity, and assume a constant radiative-subsidence speed w_r for $r > r_a$.

This paper has two main goals. The first is to derive an analytic solution for the outer wind structure model of Emanuel (2004) (Section 2), and apply this solution to accelerate the calculation of merged wind profiles (Section 3), using the merger approach of Chavas et al. (2015). This work may be of broad interest: the outer wind profile model of Emanuel (2004) is a major theoretical accomplishment that has remained under-appreciated, likely due to the lack of known closed-form solutions. The code provided as part of this work (Cronin, 2023) may also be of broad interest to researchers who model hurricane risk, as it accelerates such wind profile calculations by a factor of ~ 50, relative to the code of Chavas (2022).

The second goal is to leverage these solutions to consider how $V(r)$ may be constrained in present or future climates. I find that in the part of parameter space corresponding to real-world cyclones, merged profiles follow a scaling close to $c_D r_m V_m^2 f^{-1} \sim w_r r_0^2$, where f is the Coriolis parameter, c_D the drag coefficient, and w_r the radiative-subsidence speed (Section 4). This scaling can be justified by considering the total ascent and descent associated with the overturning circulation, and it indicates that in a future climate, storms with the same outer size will likely have a smaller radius of maximum winds due to both increases in V_m and decreases in w_r. Findings here do not rely on the analytic solution to the outer wind profile, but this section is facilitated by both faster solutions to merged profiles and also by prior discussion of the inner and outer wind solutions. Finally, I close with a summary of findings, and some thoughts about limitations and future directions (Section 5).

2 Derivation

Emanuel (2004) derives an expression for the radial gradient of the azimuthal wind (dV/dr) outside the rainy core of a Tropical cyclone, based on the angular momentum budget of the boundary-layer inflow. In steady state at a given radius, the absolute angular momentum averaged over the boundary layer depth, $M = rV + \frac{1}{2} f r^2$, is increased by inward radial advection of air with higher M, and decreased by torque due to surface stress, $c_D V^2$. Taking ψ as the cyclone's overturning circulation streamfunction in the radius-height plane at the top of the boundary layer (vertical velocity $w = \frac{1}{r}\frac{d\psi}{dr}$), this balance is:

$$\psi \frac{dM}{dr} = c_D r^2 V^2. \tag{1}$$

In the outer regions of the storm, where there are no convective updrafts, ψ must increase with decreasing radius to accommodate sinking air at the top of the boundary layer. This air is thermodynamically constrained to descend at the radiative-subsidence speed $w_r = \dot{Q}/\frac{d\theta}{dz}$, where $\dot{Q}$ is the radiative cooling rate of air just above the top of the boundary layer, and θ is the potential temperature (using the convention $w_r > 0$ for subsidence). Over Tropical oceans, radiative-subsidence speeds are typically on the order of millimeters per second, and the drag coefficient $c_D \sim 10^{-3}$. If the circulation of the storm vanishes at some outer radius, r_0, the streamfunction at $r < r_0$ can be directly obtained by integrating w_r over the annulus between r and r_0: $\psi(r) = w_r(r_0^2 - r^2)/2$ (e.g., Figure 1). This balance can equivalently be viewed as requiring a match between the Ekman suction rate at the top of the boundary layer,

$$w_{\mathrm{Ek}} = \frac{1}{r}\frac{d}{dr}\left(\frac{r c_D V^2}{f+\zeta}\right), \tag{2}$$

and the radiative-subsidence velocity, because the absolute vorticity $f+\zeta$ in the denominator of the Ekman suction can be written as $\frac{1}{r}\frac{dM}{dr}$. Either view leads to the same conclusion: the absolute angular momentum in the non-convective outer portion of the storm increases with radius according to:

$$\frac{dM}{dr} = \frac{2c_D(rV)^2}{w_r(r_0^2 - r^2)}, \tag{3}$$

which gives the following equation for V:

$$\frac{d(rV)}{dr} = \frac{2c_D(rV)^2}{w_r(r_0^2 - r^2)} - fr. \tag{4}$$

This is a Riccati equation with no known closed-form solution, but it can be transformed into a second-order ODE by a change of variables. I show below that this transformed equation is amenable to a quickly-converging power series solution when expanded in a coordinate $x \equiv 1-r/r_0$ that varies from 0 at the outer edge of the storm to 1 at storm center.

Using primes to denote derivatives of a function q with respect to r, a general Riccati equation of the form:

$$q' = A(r)q^2 + B(r) \tag{5}$$

can be rewritten as a second-order homogeneous ODE in a transformed function y, where $qA(r) = -y'/y$:

$$A(r)y'' - A'(r)y' + [A(r)]^2 B(r)y = 0. \tag{6}$$

Applying this result to Equation 4 with $q = rV$ and simplifying slightly gives:

$$(r_0^2 - r^2)y'' - 2ry' - 2\frac{c_D f}{w_r} ry = 0. \tag{7}$$

If a solution for $y(r)$ can be found, then V is given by $\frac{2c_D rV}{w_r(r_0^2-r^2)} = \frac{-y'}{y}$. I factor V into two terms:

$$V = \underbrace{\left\{\frac{f(r_0^2 - r^2)}{2r}\right\}}_{V_{AMC}(r)} \underbrace{\left[-\frac{w_r}{c_D f}\frac{y'}{y}\right]}_{G(r)}, \tag{8}$$

where the first term (in braces), labeled $V_{AMC}(r)$, is the angular-momentum-conserving azimuthal wind speed for inflow from a quiescent state at radius r_0 inward to radius r. The second term (in brackets), labeled $G(r)$, is the fractional reduction of wind speed relative to V_{AMC} due to loss of angular momentum by surface friction. Physical solutions for $G(r) \equiv -\frac{w_r}{c_D f}[y'/y]$ must be bounded on $[0, 1]$, and the appropriate boundary condition is $G(r) = 1$ at $r = r_0$. Note that since y'/y has dimensions of inverse distance, w_r distance per time, f inverse time, and c_D is dimensionless, $G(r)$ is also dimensionless.

Equation 7 can be solved with a power series in r, but this series converges slowly and has an undetermined free parameter that does not clearly relate to the outer boundary condition ($G(r) = 1$ at $r = r_0$). However, a change of variables in equation 7, to:

$$x \equiv 1 - r/r_0, \tag{9}$$

gives a power series solution that both converges comparatively quickly and easily matches the outer boundary condition. Since $dx = -dr/r_0$, Equation 7 expressed in terms of x (with an $_{(x)}$ subscript on a primed term denoting a derivative with respect to x) becomes:

$$x(2 - x)y''_{(x)} + 2(1 - x)y'_{(x)} - 2\gamma(1 - x)y = 0, \tag{10}$$

where $\gamma \equiv c_D f r_0 w_r^{-1}$ is identical to the nondimensional outer wind parameter found in Chavas and Lin (2016). Note that the solution for G is expressed in terms of $y' = dy/dr = (dy/dx)(dx/dr) = -(1/r_0)y'_{(x)}$, so $G(r) = \frac{w_r}{c_D f r_0}[y'_{(x)}/y] = \gamma^{-1}[y'_{(x)}/y]$.

The power series solution to Equation 10, given by $y = \sum_{n=0}^{\infty} a_n x^n$, can be taken generally to have $a_0 = 1$ (the choice of a_0 does not affect G since it does not alter the ratio $y'_{(x)}/y$), leading to the first few terms and recurrence relation for coefficients as follows:

$$\begin{aligned}
a_1 &= \gamma \\
a_2 &= \frac{\gamma^2}{(2!)^2} \\
a_3 &= \frac{\gamma^2(\gamma - 1)}{(3!)^2} \\
a_n &= \frac{1}{n^2}\left\{[\gamma + n(n-1)/2]a_{n-1}\right\} - \frac{1}{n^2(n-1)^2}\left\{[\gamma(n-1)^2]a_{n-2}\right\} \qquad [n > 2].
\end{aligned} \tag{11}$$

(Here, terms outside braces that are factored out show that one can write a_n as $1/(n!)^2$ multiplied by a degree-n polynomial in γ with integer coefficients – a fact used further in Text S1.) The power series of the derivative $y'_{(x)}$, is given by $y'_{(x)} = \sum_{n=0}^{\infty}(n+1)a_{n+1}x^n$, so:

$$G(r) = \frac{y'_{(x)}/\gamma}{y} \quad = \quad \frac{\sum_{n=0}^{\infty} \frac{a_{n+1}}{\gamma}(n+1)x^n}{\sum_{n=0}^{\infty} a_n x^n}$$
$$= \quad \frac{1 + \frac{\gamma}{2}x + \frac{\gamma(\gamma-1)}{12}x^2 + \ldots}{1 + \gamma x + \frac{\gamma^2}{4}x^2 + \frac{\gamma^2(\gamma-1)}{36}x^3 + \ldots}. \tag{12}$$

The last line here also shows that since $x = 0$ at $r = r_0$ this expression satisfies the outer boundary condition of $G(r) = 1$ at $r = r_0$.

The wind speed relative to the angular-momentum-conserving limit, $G(r)$, is a function of the parameter $\gamma \equiv c_D f r_0/w_r$. $G(r)$ decreases slowly with decreasing radius for small γ, and strongly with decreasing radius, particularly near $r = r_0$, for larger values of γ (Figure 2a). A larger outer radius, drag coefficient, or Coriolis parameter all correspond to a greater torque on the inflow and a greater reduction in angular momentum, whereas a larger radiative-subsidence speed leads to stronger radial advection of angular momentum by a stronger overturning circulation, and thus a weaker dependence of G on r. Real-world storms typically have $\gamma \sim 10{-}100$. No more than a few dozen terms in the series for the numerator and denominator of G are required to attain very small errors in the solution, with the required number of terms increasing with increasing γ (Figure 2b). Errors are benchmarked against a power series solution that uses 100 terms in each of the numerator and denominator. This result suggests that series solutions should be relatively efficient for calculating outer wind profiles, though more computationally efficient methods may exist. Further details of results including numerical implementation of vectorized calculation of $G(r)$ and approximate solutions to $G(r)$ are presented in Text S1 and Text S2, respectively.

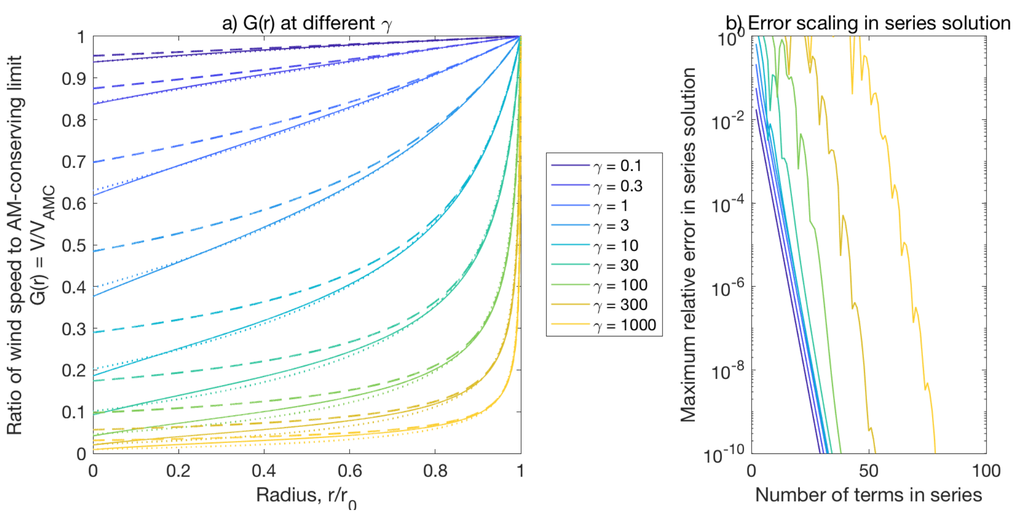

Figure 2. a) Relative azimuthal wind speed $G(r) = V(r)/V_{\mathrm{AMC}}(r)$, as a function of r/r_0, for several values of $\gamma = c_D f r_0/w_r$ (solid). Also shown are Bessel function (G_b, dashed) and empirical (G_e, dotted) approximations (Text S2). b) Dependence of maximum relative error (over $0 < r < r_0$) with the number of terms in the power series.

3 Merging with the inner wind profile

Chavas et al. (2015) merge solutions for the outer wind profile of Emanuel (2004) and the convective core wind profile of Emanuel and Rotunno (2011). I follow the same procedure, whereby V and dV/dr are matched for inner and outer profiles, but with analytic outer wind profiles in hand.

I consider the maximum azimuthal wind speed V_m and the radius of maximum winds r_m as known variables, and the merge radius between inner and outer profiles r_a and the outer radius r_0 as unknowns (r_a and r_0 are generally shown as normalized by r_m). For a ratio of enthalpy exchange to drag coefficients $c_k/c_D = 1$, the inner wind profile from Emanuel and Rotunno (2011) (their Equation 36) becomes:

$$\frac{V_{\rm in}}{V_x} = \frac{(r/r_x)}{2(V_x/fr_x)(1+(r/r_x)^2)}\left[(4(V_x/fr_x)+1)-(r/r_x)^2\right], \tag{13}$$

where $V_x \approx V_m$ and $r_x \approx r_m$. It is (unfortunately) necessary to draw a distinction between the speed V_x and radius r_x used in this expression and the "true" values of V_m and r_m, because these two are not generally identical. Equation 13 does not generally have $\max(V_{\rm in}) = V_x$ at $r = r_x$; instead this limit applies only when $V_x/(fr_x) >> 1$. The true radius of maximum winds for Equation 13, r_m, is about 5% inward of r_x when $V_x/(fr_x) = 10$, and about 0.5% inward of r_x when $V_x/(fr_x) = 100$. Correcting for this difference is necessary to get a reasonable match to previous results (Chavas, 2022) and so that the input values of V_m and r_m and the outputs from my code match. As part of the solution, several iterations are used to solve for the values of r_x and V_x in Equation 13 that give $\max(V_{\rm in}) = V_m$ at $r = r_m$.

Taking V_m and r_m as known parameters, two dimensionless variables that govern merged solutions are:

$$\tilde{w_Q} = \frac{w_r}{c_D V_m} \tag{14}$$

$$\mathrm{Ro} = \frac{V_m}{fr_m}, \tag{15}$$

where $\tilde{w_Q}$ is a normalized radiative-subsidence speed (following Emanuel, 2004; Chavas & Emanuel, 2014) that represents a ratio of the outer descent rate to the Ekman pumping ascent in the center of the storm, and Ro is the inner-core Rossby number. Although the outer wind profile has been solved analytically (Equation 12), analytic solution for the merge radius r_a and outer radius r_0 as a function of Ro and $\tilde{w_Q}$ remains infeasible. Instead, numerical solution is used: for a given (Ro, w_Q) pair, the inner wind profile is specified and the outer wind profile depends on the to-be-determined value of r_0. An iterative loop scans through several choices of r_0 to find a value that gives an outer wind profile tangent to the inner wind profile at a single point: the merge radius r_a. This follows a similar approach to Chavas and Lin (2016), but they search through slightly different variables.

The normalized outer radius r_0/r_m increases with decreasing $\tilde{w_Q}$ and increasing Ro, while the normalized merge radius r_a/r_m increases with increasing $\tilde{w_Q}$ and increasing Ro (Figure 3). The outer wind parameter, $\gamma = c_D f r_0 w_r^{-1} = (r_0/r_m)\tilde{w_Q}^{-1}\mathrm{Ro}^{-1}$, thus increases with decreasing $\tilde{w_Q}$ and Ro – unsurprising from its definition – but indicating that r_0/r_m increases sub-linearly with Ro in this parameter range. For sufficiently large $\tilde{w_Q}$, particularly at small Ro, there is no merge point and no outer wind regime at all: the inner wind profile of Emanuel and Rotunno (2011) extends to the edge of the storm (sections shaded gray in Figure 3). This matches the finding of Cronin and Chavas (2019) that wind profiles for dry hurricanes have little contribution from the outer wind regime. In Text S3, I use analytic outer wind solutions to derive an approximate bound on this subset of parameter space, and find that it corresponds roughly to the inequality:

$$\tilde{w_Q} \geq \tilde{w_Q}^* = \frac{16\mathrm{Ro}^{1/2}}{27}. \quad (16)$$

The dotted line in Figure 3 shows that this approximation generally succeeds in delimiting the part of parameter space without an outer-wind component to the merged profiles, particularly at lower Ro.

The rough position of real tropical cyclones in this joint ($\tilde{w_Q}$, Ro) parameter space in Figure 3 is indicated by colored dots for representative median storms of different intensity categories, using data from Figure 10 of Chavas et al. (2015). Colors of light gray, dark gray, green, yellow, orange, and red, respectively, indicate low-intensity Tropical Storms, high-intensity Tropical Storms, Category 1 Hurricanes, Category 2 Hurricanes, Category 3 Hurricanes, and Category 4/5 Hurricanes. Fixed values of $c_D = 0.001$ and $w_r = 0.002$ m s^{-1} are used in plotting these points. As in Chavas et al. (2015), the ratio r_0/r_m – of outer size to the radius of maximum winds – increases strongly with intensity, the normalized merge radius r_a/r_m increases weakly with intensity, and (not discussed previously) $\gamma \approx 15 - 20$ is strikingly similar across representative storms from different intensity classes. Because $\gamma = c_D f r_0/w_r$ – and f, c_D, and w_r all vary comparatively little with storm intensity – the relative constancy of γ with storm intensity is consistent with the known weak correlation between intensity and storm outer radius (e.g., Chavas & Emanuel, 2010).

Further details of methods and results for how merged wind profile calculations are performed and benchmarked against previous code (Figure S1) are presented in Text S4. By using the analytic outer wind profiles described above, together with vectorized calculations of multiple wind profiles at once and use of lookup tables for key variables (Text S1, S4), acceleration by about a factor of ~ 50 is obtained relative to the code of Chavas (2022), with comparable or greater accuracy. This corresponds to a computation time of about 10^{-4} to 10^{-3} seconds per wind profile on a single core of a laptop computer when many (> 100) profiles are computed at a time.

4 Discussion and scaling of merged profiles

In the region of parameter space characteristic of present-day Tropical cyclones ($5 <$ Ro < 50 and $0.02 < \tilde{w_Q} < 0.2$; see Figure 3), an approximate power-law fit for merged solutions is given by $r_0/r_m \sim \mathrm{Ro}^{0.5}\tilde{w_Q}^{-0.5}$. These powers are approximate and the power of Ro slightly smaller than 0.5, but this form is used because a clean approximate scaling relationship results from it among V_m, r_m, and r_0:

$$r_0 \sim r_m^{0.5} V_m f^{-0.5} c_D^{0.5} w_r^{-0.5}. \quad (17)$$

How to consider this relationship depends on which storm parameters one views as externally constrained, and which others one thus seeks to predict. In a diagnostic sense, this scaling seems promising in terms of ability to explain and in some cases reconcile seemingly disparate dependences of r_0 on sea-surface temperature, rotation rate, and surface moisture availability (Khairoutdinov & Emanuel, 2013; Zhou et al., 2014; Cronin & Chavas, 2019). Recent work on cyclone outer size, however, suggests taking the perspective that r_0, V_m, c_D, f, and w_r may all be viewed as externally constrained under future climate change (e.g., Chavas & Reed, 2019). Rearranging this expression as a scaling relationship for the radius of maximum winds then implies that r_m will likely decrease with warming for storms with the same outer size, the same or greater intensity, and in similar latitude bands. Before discussing this implication, however, it is useful to try to gain a physical understanding of Equation 17.

The wind merger condition that V and dV/dr be continuous also implies that the inner and outer streamfunctions must match at the merge radius. Equation 17 can be rearranged to emphasize this constraint that the upward mass transport in the inner region (left-hand side) must match the downward mass transport in the outer region (right-hand side):

$$c_D r_m V_m^2 f^{-1} \sim w_r r_0^2. \tag{18}$$

Note that I will use "mass transport" as a stand-in for the more accurate term "volume transport" here – reasonable if imperfect when referring to transport across the top of a cyclone's boundary layer at different radii where density may vary by $\sim$10% (the two are also implicitly equated in Emanuel, 2004). It is comparatively straightforward that the downward mass transport can be written as $w_r r_0^2$, because constant subsidence has been assumed over the annulus between r_a and r_0, and $(r_0^2 - r_a^2) \approx r_0^2$ if $r_0 >> r_a$. But why does the upward mass transport scale as $c_D r_m V_m^2 f^{-1}$? If r_a/r_m were constant, then the inner part of the storm would have upward mass transport that scaled with inner-core Ekman pumping rate, or $c_D V_m r_m^2$ (e.g., Khairoutdinov & Emanuel, 2013), yet this scaling differs slightly. Rearranging Equation 1 shows that that the overturning streamfunction can be calculated if V and M are known:

$$\psi = \frac{c_D r^2 V^2}{dM/dr}. \tag{19}$$

In Text S5 I find that this allows the integrated mass transport for the inner wind profile (Equation 13) to be approximated as:

$$\psi(r_a) = c_D V_m r_m^2 \left(\frac{r_a}{r_m}\right)^3. \tag{20}$$

If r_a/r_m depends primarily on Ro, as seen near the colored dots in Figure 3, then this may be subject to further simplification. If $r_a/r_m \sim \mathrm{Ro}^{1/3}$, then the approximate form in Equation 18 is recovered exactly. Thus, Equations 17 and 18 emerge from a combination of mass continuity, and the dependence of r_a/r_m on $\tilde{w_Q}$ and Ro – particularly the gradual increase of r_a/r_m with Ro. I know of no theoretical basis for any specific dependence of r_a/r_m on Ro, so this result highlights the importance of examining total cyclone upward mass transport in both real and simulated storms in future study. With this physical interpretation established, I consider application of Equation 18 to the question of how storm structure may change with climate warming.

Specifically, I will consider how r_m may change with warming at fixed r_0. A bit of explanation is warranted regarding this null hypothesis of constant r_0 with warming, which may surprise some readers (this hypothesis is described and substantiated further by Schenkel et al., 2023). Past studies have found mixed results regarding changes in outer size with climate warming, partly due to use of different metrics of size, and partly due to different idealizations across simulations. Simulations of cyclones on an $f-$plane often (though not universally) show an outer size that is bounded above by V_p/f (e.g., Chavas & Emanuel, 2014, where V_p is the potential intensity) – a length scale that increases with climate warming due to increasing V_p. An upper limiting "potential size" with similar scaling has also recently been given more theoretical rigor (Wang et al., 2022). The outer size of real-world cyclones, however, increases with latitude, directly counter to a $1/f$ scaling (Chavas et al., 2016). Chavas and Reed (2019) hypothesized that a crucial feature missing from $f-$plane simulations is the meridional dependence of f, or beta effect. They used numerical simulations with varied rotation rate and planetary size to show that a vortex Rhines scale $\sim (aV_\beta/(df/d\phi))^{1/2}$, where a is the planetary radius and V_β an outer circulation wind speed, likely limits cyclone size in Earth's Tropics, while a V_p/f bound may apply at higher latitudes. Critically, the vortex Rhines scale is essentially invariant with climate warming. Taken together, these results suggest that cyclones in Tropical latitudes may change little in outer size with climate warming – a result borne out by one idealized study that also shows size increases with warming at higher latitudes (e.g., Stansfield & Reed, 2021).

Thus, rearranging Equation 17, if r_0 is treated as a constant, and f also taken as fixed, r_m is expected to decrease with warming due to increasing V_m and decreasing w_r:

$$r_m \sim w_r r_0^2 f V_m^{-2} c_D^{-1}. \tag{21}$$

The radiative-subsidence speed w_r is expected to decrease modestly by $\sim 1{-}2\%$ K^{-1} with surface warming due to increases in lower-tropospheric static stability along a moist adiabat. Potential intensity is also expected to increase modestly by $\sim 1{-}2\%$ K^{-1} with surface warming (e.g., Khairoutdinov & Emanuel, 2013; Zhou et al., 2014), with changes in mean actual intensity somewhat more uncertain. Thus, expected changes in V_m and w_r combine to predict a $d\log r_m/dT \sim -5\%$ K^{-1} decrease in radius of maximum winds (at fixed f, r_0, and c_D), although some of this decrease could be offset by a poleward expansion of Tropical cyclone tracks. This leads to the hypothesis that more intense storms may have considerably smaller radii of maximum winds in a warmer climate – a result seen in some modeling studies (Chen et al., 2020; Xi et al., 2023) but worthy of deeper investigation.

5 Conclusions

The outer wind model of Emanuel (2004) has finally been analytically solved. Solutions take the form of a ratio of two power series in a normalized radius variable $x = (1-r/r_0)$ which varies between 0 at the outer edge of the storm and 1 at the storm center. The power series converge relatively quickly, and depend on one nondimensional parameter $\gamma = c_D f r_0/w_r$ (as in Chavas & Lin, 2016). The new solution is used to speed up calculations of complete wind models (merging the outer wind model of Emanuel (2004) and the inner wind model of Emanuel and Rotunno (2011) as in Chavas et al. (2015)). For merged solutions, I find that an approximate scaling relationship $r_0 \sim r_m^{0.5} V_m f^{-0.5} c_D^{0.5} w_r^{-0.5}$ holds well over the range of parameter space relevant for real Tropical cyclones. This scaling is physically consistent with constraints posed by the overturning circulation of a cyclone, together with a dependence of the size of the ascent region on the inner-core Rossby number $V_m/(f r_m)$ that is an emergent result of matching wind profiles from the two regions. If future storms have greater maximum wind speeds and a similar distribution of outer sizes (r_0), then this scaling predicts decreases in maximum wind radii with climate warming: good news.

An important result of the paper is that analytic solutions can be used to calculate merged wind profiles with considerably less computational cost than the numerical integration of Equation 3 by Chavas (2022). This may make the code developed here (Cronin, 2023) immediately useful for risk modeling and assessment. A limitation of the analytic approach, however, is that the drag coefficient, c_D, cannot be allowed to vary with wind speed as in existing numerical solutions (Chavas, 2022).

The Emanuel (2004) outer wind model is a major theoretical accomplishment, yet it has not been widely adopted by the community of researchers who study Tropical cyclones – likely due in part to the lack of a closed-form solution. I hope that the solutions provided here (and the code to implement them) spurs further adoption and testing of the validity of the outer wind model, and perhaps useful approximations of it that are simpler still to implement. A limitation of the outer wind model, especially near r_0, is that its derivation from Equation 1 has assumed a surface torque that scales as $c_D V^2$, where V is the swirling wind of the cyclone. For values of V much smaller than a background wind speed V_0, an azimuthal-mean torque $\sim c_D V_0 V$ would be more appropriate; both limits ($V >> V_0$ and $V << V_0$) can be captured by a torque $c_D V \sqrt{V_0^2 + V^2}$. I have not attempted analytic solution of Equation 1 using such a functional form, and the problem does not seem tractable by the Riccati equation solution method used above.

An extension of this work that is more analytically tractable, and possibly more useful, is the reduction in bias of the complete wind profiles by adding a third region between ascending inner and descending outer regions. Chavas et al. (2015) find that real storms deviate most from the profile of the merged model at radii somewhat greater than the merge radius. In this region, observed winds decrease less rapidly with radius than the merged model predicts, and precipitation extends well beyond r_a, violating the assumptions of the outer wind model. Analysis of the overturning circulation above suggests that the jump in assumed behavior at r_a is perhaps even more troubling than realized by Chavas et al. (2015): vertical velocities w_{in} within the inner ascending region are often maximal at r_a; this can be seen by plotting:

$$w_{\text{in}} = \frac{1}{r}\frac{d\psi_{\text{in}}}{dr} = \frac{c_D V_m (r/r_m)}{16\text{Ro}^2\left(1+\frac{1}{2\text{Ro}}\right)}\left[(4\text{Ro}+1)-(r/r_m)^2\right]\left[3(4\text{Ro}+1)-7(r/r_m)^2\right]. \quad (22)$$

Chavas et al. (2015) suggest that a natural assumption for an intermediate region would be to take $w = 0$; as a consequence ψ would be constant in the join region between inner ascending and outer descending wind profiles. This assumption replaces $(r_0^2 - r^2)$ in the denominator of Equation 4 with a constant. The resulting equation for V is solvable by the same methods I used above, and the intermediate function y is a solution to the Airy equation ($y'' - ry = 0$). Questions about the utility, uniqueness, and interpretation of such a three-region merged solution for the wind profile are left for future work.

Finally, this study has focused on a steady-state wind profile, in which radial angular momentum advection by the mean overturning circulation balances surface friction. Such a framework does not directly provide any information about how the wind profile behaves in time-evolving situations, including what might drive gradual expansion of the outer radius (e.g., Cocks & Gray, 2002; Chavas & Emanuel, 2010), more rapid changes in inner structure where r_m and V_m vary together, or the important problem of eyewall replacement cycles and secondary eyewall formation. The wind profile model will also fail in regions where other terms are important in the steady angular momentum budget, including vertical advection by the mean circulation, or convergences of eddy angular momentum fluxes in the vertical or horizontal. Nevertheless, particularly given the hypothesis that secondary eyewall formation results from a mismatch or adjustment of the inner core to the outer structure of the storm (Shivamoggi, 2022), a solid understanding of a physics-based steady wind profile seems an important foundation for building further insight into the behavior of Tropical cyclones.

Open Research Section

MATLAB code to reproduce figures in the paper and make general wind profile calculations is archived on Zenodo (doi:10.5281/zenodo.7783251, Cronin, 2023). The code version used in this paper is v20230329.

Acknowledgments

Thanks to Tom Beucler, Dan Chavas, Kerry Emanuel, and Jonathan Lin for useful exchanges about this work. I acknowledge support from the MIT Climate Grand Challenge on Weather and Climate Extremes.

References

Chavas, D. R. (2022, Jun). *Code for tropical cyclone wind profile model of Chavas et al (2015, JAS).* Retrieved from `https://purr.purdue.edu/publications/4066/1` doi: 10.4231/CZ4P-D448

Chavas, D. R., & Emanuel, K. (2014). Equilibrium tropical cyclone size in an idealized state of axisymmetric radiative–convective equilibrium. *Journal of the Atmospheric Sciences*, *71*(5), 1663–1680.

Chavas, D. R., & Emanuel, K. A. (2010). A QuikSCAT climatology of tropical cyclone size. *Geophysical Research Letters*, *37*(18), 10–13.

Chavas, D. R., & Lin, N. (2016). A model for the complete radial structure of the tropical cyclone wind field. Part II: Wind field variability. *Journal of the Atmospheric Sciences*, *73*(8), 3093-3113. doi: 10.1175/JAS-D-15-0185.1

Chavas, D. R., Lin, N., Dong, W., & Lin, Y. (2016). Observed tropical cyclone size revisited. *Journal of Climate*, *29*(8), 2923–2939.

Chavas, D. R., Lin, N., & Emanuel, K. (2015). A model for the complete radial structure of the tropical cyclone wind field. Part I: Comparison with observed structure. *Journal of the Atmospheric Sciences*, *72*(9), 3647–3662.

Chavas, D. R., & Reed, K. (2019). Dynamical aquaplanet experiments with uniform thermal forcing: System dynamics and implications for tropical cyclone genesis and size. *Journal of the Atmospheric Sciences*, *76*, 2257–2274. doi: 10.1175/JAS-D-19-0001.1

Chen, J., Wang, Z., Tam, C.-Y., Lau, N.-C., Dickson Lau, D.-S., & Mok, H.-Y. (2020). Impacts of climate change on Tropical cyclones and induced storm surges in the Pearl River Delta region using pseudo-global-warming method. *Scientific Reports*, 10:1965. doi: 10.1038/s41598-020-58824-8

Cocks, S. B., & Gray, W. M. (2002). Variability of the outer wind profiles of western North Pacific typhoons: Classifications and techniques for analysis and forecasting. *Monthly Weather Review*, *130*(8), 1989–2005.

Cronin, T. W. (2023, Mar). *Code for "An analytic model for Tropical cyclone outer winds".* Retrieved from `https://doi.org/10.5281/zenodo.7783251` doi: 10.5281/zenodo.7783251

Cronin, T. W., & Chavas, D. R. (2019). Dry and semidry tropical cyclones. *Journal of the Atmospheric Sciences*, *76*, 2193–2212. doi: 10.1175/JAS-D-18-0357.1

Emanuel, K. (2004). Tropical cyclone energetics and structure. *Atmospheric turbulence and mesoscale meteorology*(8), 165–191.

Emanuel, K., & Rotunno, R. (2011, 2012/01/04). Self-stratification of tropical cyclone outflow. Part I: Implications for storm structure. *Journal of the Atmospheric Sciences*, *68*(10), 2236–2249.

Frank, W. M. (1977). The structure and energetics of the tropical cyclone. Part I: Storm structure. *Monthly Weather Review*, *105*(9), 1119–1135.

Holland, G. J. (1980). An analytic model of the wind and pressure profiles in hurricanes. *Monthly Weather Review*, *108*(8), 1212–1218.

Irish, J. L., & Resio, D. T. (2010). A hydrodynamics-based surge scale for hurricanes. *Ocean Engineering*, *37*(1), 69–81.

Khairoutdinov, M., & Emanuel, K. (2013). Rotating radiative-convective equilibrium simulated by a cloud-resolving model. *Journal of Advances in Modeling Earth Systems*, *5*(4), 816–825.

Lin, N., & Chavas, D. (2012). On hurricane parametric wind and applications in storm surge modeling. *Journal of Geophysical Research: Atmospheres (1984–2012)*, *117*(D9).

Merrill, R. T. (1984). A comparison of large and small tropical cyclones. *Monthly Weather Review*, *112*(7), 1408–1418.

Powell, M. D., & Reinhold, T. A. (2007). Tropical cyclone destructive potential by integrated kinetic energy. *Bulletin of the American Meteorological Society*, *88*(4), 513–526.

Schenkel, B. A., Chavas, D., Lin, N., Knutson, T., Vecchi, G., & Brammer, A. (2023). North atlantic tropical cyclone outer size and structure remain unchanged by the late twenty-first century. *Journal of Climate*, *36*, 359–382. doi: 10.1175/JCLI-D-22-0066.1

Shivamoggi, R. (2022). *Secondary eyewall formation as a response to evolving tropical cyclone wind structure* (PhD Dissertation). Massachusetts Institute of Technology, Department of Earth, Atmospheric and Planetary Sciences.

Stansfield, A., & Reed, K. (2021). Tropical cyclone precipitation response to surface warming in aquaplanet simulations with uniform thermal forcing. *Journal of Geophysical Research: Atmospheres*, *126*. doi: 10.1029/2021JD035197

Wang, D., Lin, Y., & Chavas, D. R. (2022). Tropical cyclone potential size. *Journal of the Atmospheric Sciences*, *79*, 3001–3025. doi: 10.1175/JAS-D-21-0325.1

Xi, D., Lin, N., & Gori, A. (2023). Increasing sequential tropical cyclone hazards along the US East and Gulf coasts. *Nature Climate Change*, *13*, 259–265. doi: 10.1038/s41558-023-01595-7

Zhou, W., Held, I. M., & Garner, S. T. (2014). Parameter study of Tropical cyclones in rotating radiative–convective equilibrium with column physics and resolution of a 25-km GCM. *Journal of the Atmospheric Sciences*, *71*(3), 1058–1069.

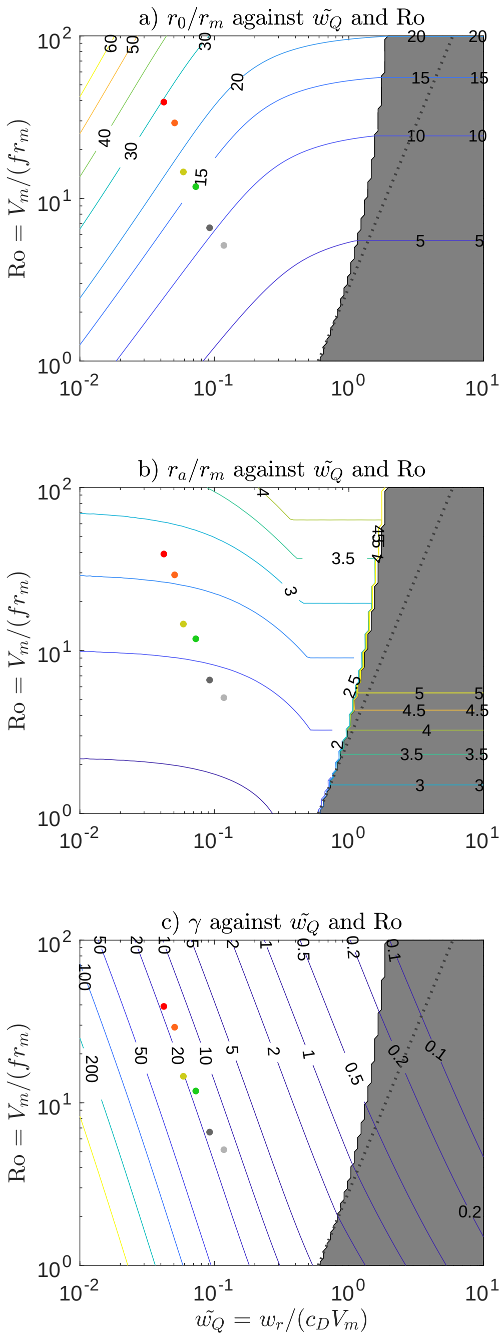

Figure 3. a) Normalized outer radius, r_0/r_m, for merged solutions as a function of nondimensional radiative-subsidence parameter $\tilde{w_Q}$ and inner core Rossby number Ro. Gray shading indicates the region of parameter space where the no outer wind solution is needed, and the black dotted line shows an approximate bound on this limit (Equation 16). Colored dots represent observed median storms from different intensity categories of Chavas et al. (2015); intensity increases from gray to red (see text for more details). b) Normalized merge radius r_a/r_m: inner solution applies for $r < r_a$ and outer solution for $r > r_a$. c) Outer wind nondimensional parameter γ.

An analytic model for Tropical cyclone outer winds

Timothy W. Cronin[1]

[1]Program in Atmospheres, Ocean, and Climate, MIT, Cambridge, Massachusetts, USA

Key Points:

- Analytic solutions are derived for the previously unsolved outer wind model of Emanuel (2004).
- Analytic wind profile calculations enable faster merged wind profile calculations, following Chavas et al. (2015).
- Scaling of merged wind profiles suggests decreases in the radius of maximum wind with warming, at constant outer size.

Corresponding author: Timothy Cronin, `twcronin@mit.edu`

Abstract

The variation of Tropical cyclone azimuthal wind speed (V) with distance from storm center (r) is a fundamental aspect of storm structure that has important implications for risk and damages. The theoretical model of Emanuel (2004), which applies well outside the rainy core of the storm, matches radiatively-driven subsidence and Ekman suction rates at the top of the boundary layer to obtain a nonlinear differential equation for dV/dr. This model is particularly appealing because of its strong physical foundation, but has no known analytic solution for $V(r)$. In this paper, I obtain an analytic solution to $V(r)$ for the Emanuel (2004) outer wind model. Following previous work, I then use this solution to explore properties of merged wind models that combine the outer model with an inner model that applies to the rainy core of a storm.

Plain Language Summary

The swirling winds of hurricanes extend far away from their centers, fading away into background weather. Previous work has proposed a theoretical model to explain how these swirling winds decrease with distance from the storm center for areas outside the rainy core of the storm. But this model has not previously been solved with pencil-and-paper methods. I find a new mathematical formula that solves the model for how winds weaken away from the center of a hurricane. I then use the solutions to examine how hurricane winds near the center of a storm relate to the winds far from the center, and what this implies about how hurricanes behave.

1 Introduction

The swirling or azimuthal winds (V) of a Tropical cyclone increase rapidly away from its calm eye to a maximum in the eyewall, then decrease much more gradually with radius (r), fading away into the background flow. This radial profile of swirling winds – which I will refer to as the "wind structure," "wind profile," or simply $V(r)$ – encapsulates important relationships among variables in a Tropical cyclone, including the maximum swirling wind speed, V_m, the radius at which these maximum winds are attained, r_m, and the far outer radius of the storm where the winds vanish, r_0. These all can influence the destructive capability of a storm, with outer size of a storm particularly important for storm surge damage (e.g., Powell & Reinhold, 2007; Irish & Resio, 2010; Lin & Chavas, 2012). For real storms, r_0 is difficult to measure directly and requires azimuthal averaging in any nonzero background flow, so Tropical cyclone size is commonly quantified using the radius of a certain fixed value of wind speed (e.g., gale-force winds) or the radius of a closed surface pressure contour, instead of the radius of vanishing winds (e.g., Frank, 1977; Merrill, 1984; Chavas & Emanuel, 2010). Numerous empirical models of wind structure have been developed and are widely used; for example, the elegant work of Holland (1980) fits the observed dependence of pressure on radius using a logarithmic rectangular hyperbola, with gradient wind balance then enabling calculation of $V(r)$. Empirical wind structure models, however, cannot identify the dynamical or kinematic constraints that might bound or link intensity, radius of maximum winds, and outer size, or provide insight on how $V(r)$ might change in a warming climate. Emanuel (2004) and Emanuel and Rotunno (2011) developed physics-based models of, respectively, storm outer and inner structure: these two were cleverly merged into a complete theoretical wind model by Chavas et al. (2015) (See schematic of merged winds in Figure 1). The inner wind model of Emanuel and Rotunno (2011) assumes a slantwise-moist-neutral core of the storm, where the radial gradients in wind speed outside the eyewall are constrained by wind shear and mixing in the outflow, and has known analytic solutions (in the limit of a cyclostrophic vortex). The outer wind model of Emanuel (2004) is based on the (sound) assumption that subsidence due to radiative cooling matches Ekman suction at the top of the boundary layer in the outer region of the storm where there is little rain and deep convection. This outer wind model, however, has been formulated only as a nonlinear differential equation for dV/dr, and lacks a known analytic solution for $V(r)$.

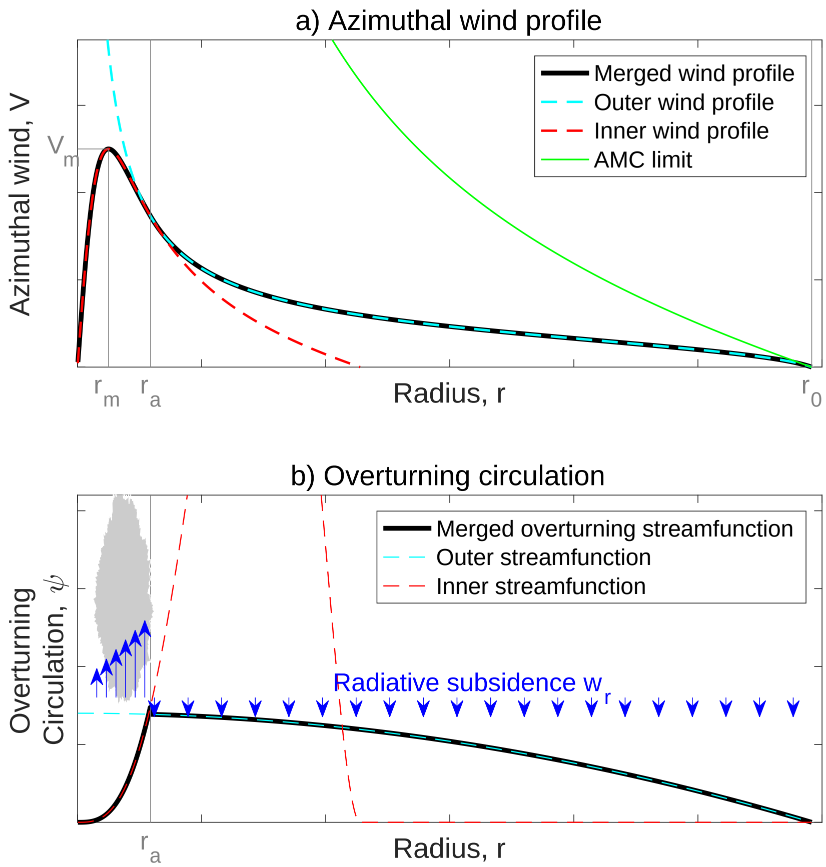

Figure 1. a) Azimuthal or swirling winds, V, of a Tropical cyclone plotted against radius, r. General features include the radius of maximum wind, r_m, the maximum wind speed V_m, and the radius of vanishing wind, r_0. The specific profile drawn in black merges the Emanuel (2004) outer wind model (cyan dashed line) and the Emanuel and Rotunno (2011) inner wind model (red dashed line), following Chavas et al. (2015). The theoretical angular-momentum-conserving wind profile (green), and the merge radius r_a are also drawn. b) The overturning circulation in the radius-height plane generally includes ascent at small radii, and sinking at large radii. Merged wind profiles of Chavas et al. (2015) have a continuous overturning streamfunction (ψ) at r_a, but a discontinuity in vertical velocity, and assume a constant radiative-subsidence speed w_r for $r > r_a$.

This paper has two main goals. The first is to derive an analytic solution for the outer wind structure model of Emanuel (2004) (Section 2), and apply this solution to accelerate the calculation of merged wind profiles (Section 3), using the merger approach of Chavas et al. (2015). This work may be of broad interest: the outer wind profile model of Emanuel (2004) is a major theoretical accomplishment that has remained under-appreciated, likely due to the lack of known closed-form solutions. The code provided as part of this work (Cronin, 2023) may also be of broad interest to researchers who model hurricane risk, as it accelerates such wind profile calculations by a factor of ~ 50, relative to the code of Chavas (2022).

The second goal is to leverage these solutions to consider how $V(r)$ may be constrained in present or future climates. I find that in the part of parameter space corresponding to real-world cyclones, merged profiles follow a scaling close to $c_D r_m V_m^2 f^{-1} \sim w_r r_0^2$, where f is the Coriolis parameter, c_D the drag coefficient, and w_r the radiative-subsidence speed (Section 4). This scaling can be justified by considering the total ascent and descent associated with the overturning circulation, and it indicates that in a future climate, storms with the same outer size will likely have a smaller radius of maximum winds due to both increases in V_m and decreases in w_r. Findings here do not rely on the analytic solution to the outer wind profile, but this section is facilitated by both faster solutions to merged profiles and also by prior discussion of the inner and outer wind solutions. Finally, I close with a summary of findings, and some thoughts about limitations and future directions (Section 5).

2 Derivation

Emanuel (2004) derives an expression for the radial gradient of the azimuthal wind (dV/dr) outside the rainy core of a Tropical cyclone, based on the angular momentum budget of the boundary-layer inflow. In steady state at a given radius, the absolute angular momentum averaged over the boundary layer depth, $M = rV + \frac{1}{2} f r^2$, is increased by inward radial advection of air with higher M, and decreased by torque due to surface stress, $c_D V^2$. Taking ψ as the cyclone's overturning circulation streamfunction in the radius-height plane at the top of the boundary layer (vertical velocity $w = \frac{1}{r}\frac{d\psi}{dr}$), this balance is:

$$\psi \frac{dM}{dr} = c_D r^2 V^2. \tag{1}$$

In the outer regions of the storm, where there are no convective updrafts, ψ must increase with decreasing radius to accommodate sinking air at the top of the boundary layer. This air is thermodynamically constrained to descend at the radiative-subsidence speed $w_r = \dot{Q}/\frac{d\theta}{dz}$, where $\dot{Q}$ is the radiative cooling rate of air just above the top of the boundary layer, and θ is the potential temperature (using the convention $w_r > 0$ for subsidence). Over Tropical oceans, radiative-subsidence speeds are typically on the order of millimeters per second, and the drag coefficient $c_D \sim 10^{-3}$. If the circulation of the storm vanishes at some outer radius, r_0, the streamfunction at $r < r_0$ can be directly obtained by integrating w_r over the annulus between r and r_0: $\psi(r) = w_r(r_0^2 - r^2)/2$ (e.g., Figure 1). This balance can equivalently be viewed as requiring a match between the Ekman suction rate at the top of the boundary layer,

$$w_{\mathrm{Ek}} = \frac{1}{r}\frac{d}{dr}\left(\frac{r c_D V^2}{f+\zeta}\right), \tag{2}$$

and the radiative-subsidence velocity, because the absolute vorticity $f+\zeta$ in the denominator of the Ekman suction can be written as $\frac{1}{r}\frac{dM}{dr}$. Either view leads to the same conclusion: the absolute angular momentum in the non-convective outer portion of the storm increases with radius according to:

$$\frac{dM}{dr} = \frac{2c_D (rV)^2}{w_r(r_0^2 - r^2)}, \tag{3}$$

which gives the following equation for V:

$$\frac{d(rV)}{dr} = \frac{2c_D (rV)^2}{w_r(r_0^2 - r^2)} - fr. \tag{4}$$

This is a Riccati equation with no known closed-form solution, but it can be transformed into a second-order ODE by a change of variables. I show below that this transformed equation is amenable to a quickly-converging power series solution when expanded in a coordinate $x \equiv 1-r/r_0$ that varies from 0 at the outer edge of the storm to 1 at storm center.

Using primes to denote derivatives of a function q with respect to r, a general Riccati equation of the form:

$$q' = A(r)q^2 + B(r) \tag{5}$$

can be rewritten as a second-order homogeneous ODE in a transformed function y, where $qA(r) = -y'/y$:

$$A(r)y'' - A'(r)y' + [A(r)]^2 B(r)y = 0. \tag{6}$$

Applying this result to Equation 4 with $q = rV$ and simplifying slightly gives:

$$(r_0^2 - r^2)y'' - 2ry' - 2\frac{c_D f}{w_r} ry = 0. \tag{7}$$

If a solution for $y(r)$ can be found, then V is given by $\frac{2c_D rV}{w_r(r_0^2-r^2)} = \frac{-y'}{y}$. I factor V into two terms:

$$V = \underbrace{\left\{\frac{f(r_0^2 - r^2)}{2r}\right\}}_{V_{AMC}(r)} \underbrace{\left[-\frac{w_r}{c_D f}\frac{y'}{y}\right]}_{G(r)}, \tag{8}$$

where the first term (in braces), labeled $V_{AMC}(r)$, is the angular-momentum-conserving azimuthal wind speed for inflow from a quiescent state at radius r_0 inward to radius r. The second term (in brackets), labeled $G(r)$, is the fractional reduction of wind speed relative to V_{AMC} due to loss of angular momentum by surface friction. Physical solutions for $G(r) \equiv -\frac{w_r}{c_D f}[y'/y]$ must be bounded on $[0, 1]$, and the appropriate boundary condition is $G(r) = 1$ at $r = r_0$. Note that since y'/y has dimensions of inverse distance, w_r distance per time, f inverse time, and c_D is dimensionless, $G(r)$ is also dimensionless.

Equation 7 can be solved with a power series in r, but this series converges slowly and has an undetermined free parameter that does not clearly relate to the outer boundary condition ($G(r) = 1$ at $r = r_0$). However, a change of variables in equation 7, to:

$$x \equiv 1 - r/r_0, \tag{9}$$

gives a power series solution that both converges comparatively quickly and easily matches the outer boundary condition. Since $dx = -dr/r_0$, Equation 7 expressed in terms of x (with an $_{(x)}$ subscript on a primed term denoting a derivative with respect to x) becomes:

$$x(2 - x)y''_{(x)} + 2(1 - x)y'_{(x)} - 2\gamma(1 - x)y = 0, \tag{10}$$

where $\gamma \equiv c_D f r_0 w_r^{-1}$ is identical to the nondimensional outer wind parameter found in Chavas and Lin (2016). Note that the solution for G is expressed in terms of $y' = dy/dr = (dy/dx)(dx/dr) = -(1/r_0)y'_{(x)}$, so $G(r) = \frac{w_r}{c_D f r_0}[y'_{(x)}/y] = \gamma^{-1}[y'_{(x)}/y]$.

The power series solution to Equation 10, given by $y = \sum_{n=0}^{\infty} a_n x^n$, can be taken generally to have $a_0 = 1$ (the choice of a_0 does not affect G since it does not alter the ratio $y'_{(x)}/y$), leading to the first few terms and recurrence relation for coefficients as follows:

$$\begin{aligned}
a_1 &= \gamma \\
a_2 &= \frac{\gamma^2}{(2!)^2} \\
a_3 &= \frac{\gamma^2(\gamma - 1)}{(3!)^2} \\
a_n &= \frac{1}{n^2}\left\{[\gamma + n(n-1)/2]a_{n-1}\right\} - \frac{1}{n^2(n-1)^2}\left\{[\gamma(n-1)^2]a_{n-2}\right\} \qquad [n > 2].
\end{aligned} \tag{11}$$

(Here, terms outside braces that are factored out show that one can write a_n as $1/(n!)^2$ multiplied by a degree-n polynomial in γ with integer coefficients – a fact used further in Text S1.) The power series of the derivative $y'_{(x)}$, is given by $y'_{(x)} = \sum_{n=0}^{\infty}(n+1)a_{n+1}x^n$, so:

$$
\begin{aligned}
G(r) = \frac{y'_{(x)}/\gamma}{y} &= \frac{\sum_{n=0}^{\infty}\frac{a_{n+1}}{\gamma}(n+1)x^n}{\sum_{n=0}^{\infty}a_n x^n} \\
&= \frac{1+\frac{\gamma}{2}x+\frac{\gamma(\gamma-1)}{12}x^2+\ldots}{1+\gamma x+\frac{\gamma^2}{4}x^2+\frac{\gamma^2(\gamma-1)}{36}x^3+\ldots}.
\end{aligned} \tag{12}
$$

The last line here also shows that since $x = 0$ at $r = r_0$ this expression satisfies the outer boundary condition of $G(r) = 1$ at $r = r_0$.

The wind speed relative to the angular-momentum-conserving limit, $G(r)$, is a function of the parameter $\gamma \equiv c_D f r_0/w_r$. $G(r)$ decreases slowly with decreasing radius for small γ, and strongly with decreasing radius, particularly near $r = r_0$, for larger values of γ (Figure 2a). A larger outer radius, drag coefficient, or Coriolis parameter all correspond to a greater torque on the inflow and a greater reduction in angular momentum, whereas a larger radiative-subsidence speed leads to stronger radial advection of angular momentum by a stronger overturning circulation, and thus a weaker dependence of G on r. Real-world storms typically have $\gamma \sim 10-100$. No more than a few dozen terms in the series for the numerator and denominator of G are required to attain very small errors in the solution, with the required number of terms increasing with increasing γ (Figure 2b). Errors are benchmarked against a power series solution that uses 100 terms in each of the numerator and denominator. This result suggests that series solutions should be relatively efficient for calculating outer wind profiles, though more computationally efficient methods may exist. Further details of results including numerical implementation of vectorized calculation of $G(r)$ and approximate solutions to $G(r)$ are presented in Text S1 and Text S2, respectively.

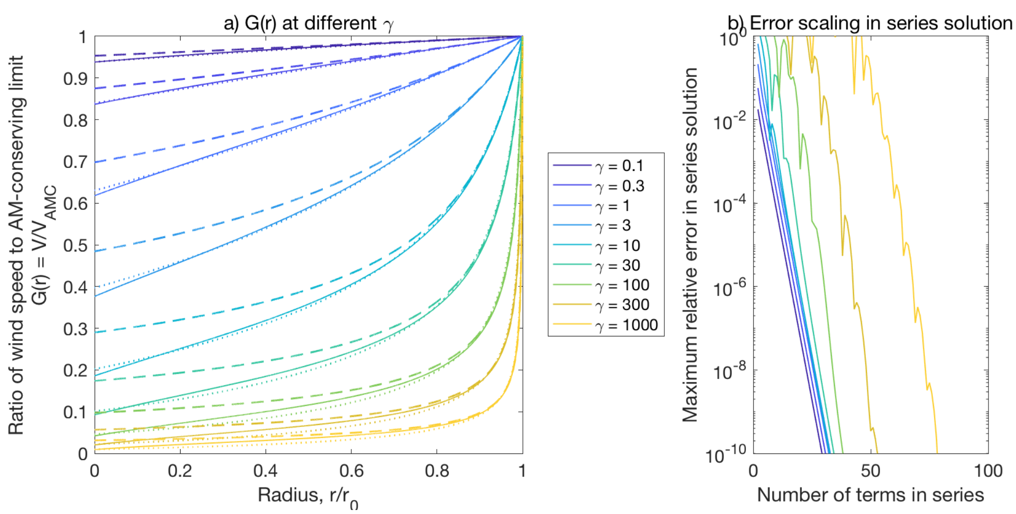

Figure 2. a) Relative azimuthal wind speed $G(r) = V(r)/V_{\mathrm{AMC}}(r)$, as a function of r/r_0, for several values of $\gamma = c_D f r_0/w_r$ (solid). Also shown are Bessel function (G_b, dashed) and empirical (G_e, dotted) approximations (Text S2). b) Dependence of maximum relative error (over $0 < r < r_0$) with the number of terms in the power series.

3 Merging with the inner wind profile

Chavas et al. (2015) merge solutions for the outer wind profile of Emanuel (2004) and the convective core wind profile of Emanuel and Rotunno (2011). I follow the same procedure, whereby V and dV/dr are matched for inner and outer profiles, but with analytic outer wind profiles in hand.

I consider the maximum azimuthal wind speed V_m and the radius of maximum winds r_m as known variables, and the merge radius between inner and outer profiles r_a and the outer radius r_0 as unknowns (r_a and r_0 are generally shown as normalized by r_m). For a ratio of enthalpy exchange to drag coefficients $c_k/c_D = 1$, the inner wind profile from Emanuel and Rotunno (2011) (their Equation 36) becomes:

$$\frac{V_{\text{in}}}{V_x} = \frac{(r/r_x)}{2(V_x/fr_x)(1+(r/r_x)^2)}\left[(4(V_x/fr_x)+1)-(r/r_x)^2\right], \tag{13}$$

where $V_x \approx V_m$ and $r_x \approx r_m$. It is (unfortunately) necessary to draw a distinction between the speed V_x and radius r_x used in this expression and the "true" values of V_m and r_m, because these two are not generally identical. Equation 13 does not generally have $\max(V_{\text{in}}) = V_x$ at $r = r_x$; instead this limit applies only when $V_x/(fr_x) >> 1$. The true radius of maximum winds for Equation 13, r_m, is about 5% inward of r_x when $V_x/(fr_x) = 10$, and about 0.5% inward of r_x when $V_x/(fr_x) = 100$. Correcting for this difference is necessary to get a reasonable match to previous results (Chavas, 2022) and so that the input values of V_m and r_m and the outputs from my code match. As part of the solution, several iterations are used to solve for the values of r_x and V_x in Equation 13 that give $\max(V_{\text{in}}) = V_m$ at $r = r_m$.

Taking V_m and r_m as known parameters, two dimensionless variables that govern merged solutions are:

$$\tilde{w_Q} = \frac{w_r}{c_D V_m} \tag{14}$$

$$\text{Ro} = \frac{V_m}{fr_m}, \tag{15}$$

where $\tilde{w_Q}$ is a normalized radiative-subsidence speed (following Emanuel, 2004; Chavas & Emanuel, 2014) that represents a ratio of the outer descent rate to the Ekman pumping ascent in the center of the storm, and Ro is the inner-core Rossby number. Although the outer wind profile has been solved analytically (Equation 12), analytic solution for the merge radius r_a and outer radius r_0 as a function of Ro and $\tilde{w_Q}$ remains infeasible. Instead, numerical solution is used: for a given (Ro, w_Q) pair, the inner wind profile is specified and the outer wind profile depends on the to-be-determined value of r_0. An iterative loop scans through several choices of r_0 to find a value that gives an outer wind profile tangent to the inner wind profile at a single point: the merge radius r_a. This follows a similar approach to Chavas and Lin (2016), but they search through slightly different variables.

The normalized outer radius r_0/r_m increases with decreasing $\tilde{w_Q}$ and increasing Ro, while the normalized merge radius r_a/r_m increases with increasing $\tilde{w_Q}$ and increasing Ro (Figure 3). The outer wind parameter, $\gamma = c_D f r_0 w_r^{-1} = (r_0/r_m)\tilde{w_Q}^{-1}\text{Ro}^{-1}$, thus increases with decreasing $\tilde{w_Q}$ and Ro – unsurprising from its definition – but indicating that r_0/r_m increases sub-linearly with Ro in this parameter range. For sufficiently large $\tilde{w_Q}$, particularly at small Ro, there is no merge point and no outer wind regime at all: the inner wind profile of Emanuel and Rotunno (2011) extends to the edge of the storm (sections shaded gray in Figure 3). This matches the finding of Cronin and Chavas (2019) that wind profiles for dry hurricanes have little contribution from the outer wind regime. In Text S3, I use analytic outer wind solutions to derive an approximate bound on this subset of parameter space, and find that it corresponds roughly to the inequality:

$$\tilde{w_Q} \geq \tilde{w_Q}^* = \frac{16\mathrm{Ro}^{1/2}}{27}. \tag{16}$$

The dotted line in Figure 3 shows that this approximation generally succeeds in delimiting the part of parameter space without an outer-wind component to the merged profiles, particularly at lower Ro.

The rough position of real tropical cyclones in this joint $(\tilde{w_Q}, \mathrm{Ro})$ parameter space in Figure 3 is indicated by colored dots for representative median storms of different intensity categories, using data from Figure 10 of Chavas et al. (2015). Colors of light gray, dark gray, green, yellow, orange, and red, respectively, indicate low-intensity Tropical Storms, high-intensity Tropical Storms, Category 1 Hurricanes, Category 2 Hurricanes, Category 3 Hurricanes, and Category 4/5 Hurricanes. Fixed values of $c_D = 0.001$ and $w_r = 0.002$ m s^{-1} are used in plotting these points. As in Chavas et al. (2015), the ratio r_0/r_m – of outer size to the radius of maximum winds – increases strongly with intensity, the normalized merge radius r_a/r_m increases weakly with intensity, and (not discussed previously) $\gamma \approx 15 - 20$ is strikingly similar across representative storms from different intensity classes. Because $\gamma = c_D f r_0/w_r$ – and f, c_D, and w_r all vary comparatively little with storm intensity – the relative constancy of γ with storm intensity is consistent with the known weak correlation between intensity and storm outer radius (e.g., Chavas & Emanuel, 2010).

Further details of methods and results for how merged wind profile calculations are performed and benchmarked against previous code (Figure S1) are presented in Text S4. By using the analytic outer wind profiles described above, together with vectorized calculations of multiple wind profiles at once and use of lookup tables for key variables (Text S1, S4), acceleration by about a factor of ~ 50 is obtained relative to the code of Chavas (2022), with comparable or greater accuracy. This corresponds to a computation time of about 10^{-4} to 10^{-3} seconds per wind profile on a single core of a laptop computer when many (> 100) profiles are computed at a time.

4 Discussion and scaling of merged profiles

In the region of parameter space characteristic of present-day Tropical cyclones ($5 < \mathrm{Ro} < 50$ and $0.02 < \tilde{w_Q} < 0.2$; see Figure 3), an approximate power-law fit for merged solutions is given by $r_0/r_m \sim \mathrm{Ro}^{0.5}\tilde{w_Q}^{-0.5}$. These powers are approximate and the power of Ro slightly smaller than 0.5, but this form is used because a clean approximate scaling relationship results from it among V_m, r_m, and r_0:

$$r_0 \sim r_m^{0.5} V_m f^{-0.5} c_D^{0.5} w_r^{-0.5}. \tag{17}$$

How to consider this relationship depends on which storm parameters one views as externally constrained, and which others one thus seeks to predict. In a diagnostic sense, this scaling seems promising in terms of ability to explain and in some cases reconcile seemingly disparate dependences of r_0 on sea-surface temperature, rotation rate, and surface moisture availability (Khairoutdinov & Emanuel, 2013; Zhou et al., 2014; Cronin & Chavas, 2019). Recent work on cyclone outer size, however, suggests taking the perspective that r_0, V_m, c_D, f, and w_r may all be viewed as externally constrained under future climate change (e.g., Chavas & Reed, 2019). Rearranging this expression as a scaling relationship for the radius of maximum winds then implies that r_m will likely decrease with warming for storms with the same outer size, the same or greater intensity, and in similar latitude bands. Before discussing this implication, however, it is useful to try to gain a physical understanding of Equation 17.

The wind merger condition that V and dV/dr be continuous also implies that the inner and outer streamfunctions must match at the merge radius. Equation 17 can be rearranged to emphasize this constraint that the upward mass transport in the inner region (left-hand side) must match the downward mass transport in the outer region (right-hand side):

$$c_D r_m V_m^2 f^{-1} \sim w_r r_0^2. \tag{18}$$

Note that I will use "mass transport" as a stand-in for the more accurate term "volume transport" here – reasonable if imperfect when referring to transport across the top of a cyclone's boundary layer at different radii where density may vary by $\sim$10% (the two are also implicitly equated in Emanuel, 2004). It is comparatively straightforward that the downward mass transport can be written as $w_r r_0^2$, because constant subsidence has been assumed over the annulus between r_a and r_0, and $(r_0^2 - r_a^2) \approx r_0^2$ if $r_0 >> r_a$. But why does the upward mass transport scale as $c_D r_m V_m^2 f^{-1}$? If r_a/r_m were constant, then the inner part of the storm would have upward mass transport that scaled with inner-core Ekman pumping rate, or $c_D V_m r_m^2$ (e.g., Khairoutdinov & Emanuel, 2013), yet this scaling differs slightly. Rearranging Equation 1 shows that that the overturning streamfunction can be calculated if V and M are known:

$$\psi = \frac{c_D r^2 V^2}{dM/dr}. \tag{19}$$

In Text S5 I find that this allows the integrated mass transport for the inner wind profile (Equation 13) to be approximated as:

$$\psi(r_a) = c_D V_m r_m^2 \left(\frac{r_a}{r_m}\right)^3. \tag{20}$$

If r_a/r_m depends primarily on Ro, as seen near the colored dots in Figure 3, then this may be subject to further simplification. If $r_a/r_m \sim \mathrm{Ro}^{1/3}$, then the approximate form in Equation 18 is recovered exactly. Thus, Equations 17 and 18 emerge from a combination of mass continuity, and the dependence of r_a/r_m on $\tilde{w_Q}$ and Ro – particularly the gradual increase of r_a/r_m with Ro. I know of no theoretical basis for any specific dependence of r_a/r_m on Ro, so this result highlights the importance of examining total cyclone upward mass transport in both real and simulated storms in future study. With this physical interpretation established, I consider application of Equation 18 to the question of how storm structure may change with climate warming.

Specifically, I will consider how r_m may change with warming at fixed r_0. A bit of explanation is warranted regarding this null hypothesis of constant r_0 with warming, which may surprise some readers (this hypothesis is described and substantiated further by Schenkel et al., 2023). Past studies have found mixed results regarding changes in outer size with climate warming, partly due to use of different metrics of size, and partly due to different idealizations across simulations. Simulations of cyclones on an $f-$plane often (though not universally) show an outer size that is bounded above by V_p/f (e.g., Chavas & Emanuel, 2014, where V_p is the potential intensity) – a length scale that increases with climate warming due to increasing V_p. An upper limiting "potential size" with similar scaling has also recently been given more theoretical rigor (Wang et al., 2022). The outer size of real-world cyclones, however, increases with latitude, directly counter to a $1/f$ scaling (Chavas et al., 2016). Chavas and Reed (2019) hypothesized that a crucial feature missing from $f-$plane simulations is the meridional dependence of f, or beta effect. They used numerical simulations with varied rotation rate and planetary size to show that a vortex Rhines scale $\sim (aV_\beta/(df/d\phi))^{1/2}$, where a is the planetary radius and V_β an outer circulation wind speed, likely limits cyclone size in Earth's Tropics, while a V_p/f bound may apply at higher latitudes. Critically, the vortex Rhines scale is essentially invariant with climate warming. Taken together, these results suggest that cyclones in Tropical latitudes may change little in outer size with climate warming – a result borne out by one idealized study that also shows size increases with warming at higher latitudes (e.g., Stansfield & Reed, 2021).

Thus, rearranging Equation 17, if r_0 is treated as a constant, and f also taken as fixed, r_m is expected to decrease with warming due to increasing V_m and decreasing w_r:

$$r_m \sim w_r r_0^2 f V_m^{-2} c_D^{-1}. \tag{21}$$

The radiative-subsidence speed w_r is expected to decrease modestly by $\sim 1{-}2\%\ \mathrm{K}^{-1}$ with surface warming due to increases in lower-tropospheric static stability along a moist adiabat. Potential intensity is also expected to increase modestly by $\sim 1{-}2\%\ \mathrm{K}^{-1}$ with surface warming (e.g., Khairoutdinov & Emanuel, 2013; Zhou et al., 2014), with changes in mean actual intensity somewhat more uncertain. Thus, expected changes in V_m and w_r combine to predict a $d \log r_m/dT \sim -5\%\ \mathrm{K}^{-1}$ decrease in radius of maximum winds (at fixed f, r_0, and c_D), although some of this decrease could be offset by a poleward expansion of Tropical cyclone tracks. This leads to the hypothesis that more intense storms may have considerably smaller radii of maximum winds in a warmer climate – a result seen in some modeling studies (Chen et al., 2020; Xi et al., 2023) but worthy of deeper investigation.

5 Conclusions

The outer wind model of Emanuel (2004) has finally been analytically solved. Solutions take the form of a ratio of two power series in a normalized radius variable $x = (1-r/r_0)$ which varies between 0 at the outer edge of the storm and 1 at the storm center. The power series converge relatively quickly, and depend on one nondimensional parameter $\gamma = c_D f r_0/w_r$ (as in Chavas & Lin, 2016). The new solution is used to speed up calculations of complete wind models (merging the outer wind model of Emanuel (2004) and the inner wind model of Emanuel and Rotunno (2011) as in Chavas et al. (2015)). For merged solutions, I find that an approximate scaling relationship $r_0 \sim r_m^{0.5} V_m f^{-0.5} c_D^{0.5} w_r^{-0.5}$ holds well over the range of parameter space relevant for real Tropical cyclones. This scaling is physically consistent with constraints posed by the overturning circulation of a cyclone, together with a dependence of the size of the ascent region on the inner-core Rossby number $V_m/(f r_m)$ that is an emergent result of matching wind profiles from the two regions. If future storms have greater maximum wind speeds and a similar distribution of outer sizes (r_0), then this scaling predicts decreases in maximum wind radii with climate warming: good news.

An important result of the paper is that analytic solutions can be used to calculate merged wind profiles with considerably less computational cost than the numerical integration of Equation 3 by Chavas (2022). This may make the code developed here (Cronin, 2023) immediately useful for risk modeling and assessment. A limitation of the analytic approach, however, is that the drag coefficient, c_D, cannot be allowed to vary with wind speed as in existing numerical solutions (Chavas, 2022).

The Emanuel (2004) outer wind model is a major theoretical accomplishment, yet it has not been widely adopted by the community of researchers who study Tropical cyclones – likely due in part to the lack of a closed-form solution. I hope that the solutions provided here (and the code to implement them) spurs further adoption and testing of the validity of the outer wind model, and perhaps useful approximations of it that are simpler still to implement. A limitation of the outer wind model, especially near r_0, is that its derivation from Equation 1 has assumed a surface torque that scales as $c_D V^2$, where V is the swirling wind of the cyclone. For values of V much smaller than a background wind speed V_0, an azimuthal-mean torque $\sim c_D V_0 V$ would be more appropriate; both limits ($V >> V_0$ and $V << V_0$) can be captured by a torque $c_D V \sqrt{V_0^2 + V^2}$. I have not attempted analytic solution of Equation 1 using such a functional form, and the problem does not seem tractable by the Riccati equation solution method used above.

An extension of this work that is more analytically tractable, and possibly more useful, is the reduction in bias of the complete wind profiles by adding a third region between ascending inner and descending outer regions. Chavas et al. (2015) find that real storms deviate most from the profile of the merged model at radii somewhat greater than the merge radius. In this region, observed winds decrease less rapidly with radius than the merged model predicts, and precipitation extends well beyond r_a, violating the assumptions of the outer wind model. Analysis of the overturning circulation above suggests that the jump in assumed behavior at r_a is perhaps even more troubling than realized by Chavas et al. (2015): vertical velocities w_{in} within the inner ascending region are often maximal at r_a; this can be seen by plotting:

$$w_{\text{in}} = \frac{1}{r}\frac{d\psi_{\text{in}}}{dr} = \frac{c_D V_m (r/r_m)}{16\text{Ro}^2\left(1+\frac{1}{2\text{Ro}}\right)}\left[(4\text{Ro}+1)-(r/r_m)^2\right]\left[3(4\text{Ro}+1)-7(r/r_m)^2\right]. \quad (22)$$

Chavas et al. (2015) suggest that a natural assumption for an intermediate region would be to take $w = 0$; as a consequence ψ would be constant in the join region between inner ascending and outer descending wind profiles. This assumption replaces $(r_0^2 - r^2)$ in the denominator of Equation 4 with a constant. The resulting equation for V is solvable by the same methods I used above, and the intermediate function y is a solution to the Airy equation ($y'' - ry = 0$). Questions about the utility, uniqueness, and interpretation of such a three-region merged solution for the wind profile are left for future work.

Finally, this study has focused on a steady-state wind profile, in which radial angular momentum advection by the mean overturning circulation balances surface friction. Such a framework does not directly provide any information about how the wind profile behaves in time-evolving situations, including what might drive gradual expansion of the outer radius (e.g., Cocks & Gray, 2002; Chavas & Emanuel, 2010), more rapid changes in inner structure where r_m and V_m vary together, or the important problem of eyewall replacement cycles and secondary eyewall formation. The wind profile model will also fail in regions where other terms are important in the steady angular momentum budget, including vertical advection by the mean circulation, or convergences of eddy angular momentum fluxes in the vertical or horizontal. Nevertheless, particularly given the hypothesis that secondary eyewall formation results from a mismatch or adjustment of the inner core to the outer structure of the storm (Shivamoggi, 2022), a solid understanding of a physics-based steady wind profile seems an important foundation for building further insight into the behavior of Tropical cyclones.

Open Research Section

MATLAB code to reproduce figures in the paper and make general wind profile calculations is archived on Zenodo (doi:10.5281/zenodo.7783251, Cronin, 2023). The code version used in this paper is v20230329.

Acknowledgments

Thanks to Tom Beucler, Dan Chavas, Kerry Emanuel, and Jonathan Lin for useful exchanges about this work. I acknowledge support from the MIT Climate Grand Challenge on Weather and Climate Extremes.

References

Chavas, D. R. (2022, Jun). *Code for tropical cyclone wind profile model of Chavas et al (2015, JAS).* Retrieved from `https://purr.purdue.edu/publications/4066/1` doi: 10.4231/CZ4P-D448

Chavas, D. R., & Emanuel, K. (2014). Equilibrium tropical cyclone size in an idealized state of axisymmetric radiative–convective equilibrium. *Journal of the Atmospheric Sciences*, *71*(5), 1663–1680.

Chavas, D. R., & Emanuel, K. A. (2010). A QuikSCAT climatology of tropical cyclone size. *Geophysical Research Letters*, *37*(18), 10–13.

Chavas, D. R., & Lin, N. (2016). A model for the complete radial structure of the tropical cyclone wind field. Part II: Wind field variability. *Journal of the Atmospheric Sciences*, *73*(8), 3093-3113. doi: 10.1175/JAS-D-15-0185.1

Chavas, D. R., Lin, N., Dong, W., & Lin, Y. (2016). Observed tropical cyclone size revisited. *Journal of Climate*, *29*(8), 2923–2939.

Chavas, D. R., Lin, N., & Emanuel, K. (2015). A model for the complete radial structure of the tropical cyclone wind field. Part I: Comparison with observed structure. *Journal of the Atmospheric Sciences*, *72*(9), 3647–3662.

Chavas, D. R., & Reed, K. (2019). Dynamical aquaplanet experiments with uniform thermal forcing: System dynamics and implications for tropical cyclone genesis and size. *Journal of the Atmospheric Sciences*, *76*, 2257–2274. doi: 10.1175/JAS-D-19-0001.1

Chen, J., Wang, Z., Tam, C.-Y., Lau, N.-C., Dickson Lau, D.-S., & Mok, H.-Y. (2020). Impacts of climate change on Tropical cyclones and induced storm surges in the Pearl River Delta region using pseudo-global-warming method. *Scientific Reports*, 10:1965. doi: 10.1038/s41598-020-58824-8

Cocks, S. B., & Gray, W. M. (2002). Variability of the outer wind profiles of western North Pacific typhoons: Classifications and techniques for analysis and forecasting. *Monthly Weather Review*, *130*(8), 1989–2005.

Cronin, T. W. (2023, Mar). *Code for "An analytic model for Tropical cyclone outer winds".* Retrieved from `https://doi.org/10.5281/zenodo.7783251` doi: 10.5281/zenodo.7783251

Cronin, T. W., & Chavas, D. R. (2019). Dry and semidry tropical cyclones. *Journal of the Atmospheric Sciences*, *76*, 2193–2212. doi: 10.1175/JAS-D-18-0357.1

Emanuel, K. (2004). Tropical cyclone energetics and structure. *Atmospheric turbulence and mesoscale meteorology*(8), 165–191.

Emanuel, K., & Rotunno, R. (2011, 2012/01/04). Self-stratification of tropical cyclone outflow. Part I: Implications for storm structure. *Journal of the Atmospheric Sciences*, *68*(10), 2236–2249.

Frank, W. M. (1977). The structure and energetics of the tropical cyclone. Part I: Storm structure. *Monthly Weather Review*, *105*(9), 1119–1135.

Holland, G. J. (1980). An analytic model of the wind and pressure profiles in hurricanes. *Monthly Weather Review*, *108*(8), 1212–1218.

Irish, J. L., & Resio, D. T. (2010). A hydrodynamics-based surge scale for hurricanes. *Ocean Engineering*, *37*(1), 69–81.

Khairoutdinov, M., & Emanuel, K. (2013). Rotating radiative-convective equilibrium simulated by a cloud-resolving model. *Journal of Advances in Modeling Earth Systems*, *5*(4), 816–825.

Lin, N., & Chavas, D. (2012). On hurricane parametric wind and applications in storm surge modeling. *Journal of Geophysical Research: Atmospheres (1984–2012)*, *117*(D9).

Merrill, R. T. (1984). A comparison of large and small tropical cyclones. *Monthly Weather Review*, *112*(7), 1408–1418.

Powell, M. D., & Reinhold, T. A. (2007). Tropical cyclone destructive potential by integrated kinetic energy. *Bulletin of the American Meteorological Society*, *88*(4), 513–526.

Schenkel, B. A., Chavas, D., Lin, N., Knutson, T., Vecchi, G., & Brammer, A. (2023). North atlantic tropical cyclone outer size and structure remain unchanged by the late twenty-first century. *Journal of Climate*, *36*, 359–382. doi: 10.1175/JCLI-D-22-0066.1

Shivamoggi, R. (2022). *Secondary eyewall formation as a response to evolving tropical cyclone wind structure* (PhD Dissertation). Massachusetts Institute of Technology, Department of Earth, Atmospheric and Planetary Sciences.

Stansfield, A., & Reed, K. (2021). Tropical cyclone precipitation response to surface warming in aquaplanet simulations with uniform thermal forcing. *Journal of Geophysical Research: Atmospheres*, *126*. doi: 10.1029/2021JD035197

Wang, D., Lin, Y., & Chavas, D. R. (2022). Tropical cyclone potential size. *Journal of the Atmospheric Sciences*, *79*, 3001–3025. doi: 10.1175/JAS-D-21-0325.1

Xi, D., Lin, N., & Gori, A. (2023). Increasing sequential tropical cyclone hazards along the US East and Gulf coasts. *Nature Climate Change*, *13*, 259–265. doi: 10.1038/s41558-023-01595-7

Zhou, W., Held, I. M., & Garner, S. T. (2014). Parameter study of Tropical cyclones in rotating radiative–convective equilibrium with column physics and resolution of a 25-km GCM. *Journal of the Atmospheric Sciences*, *71*(3), 1058–1069.

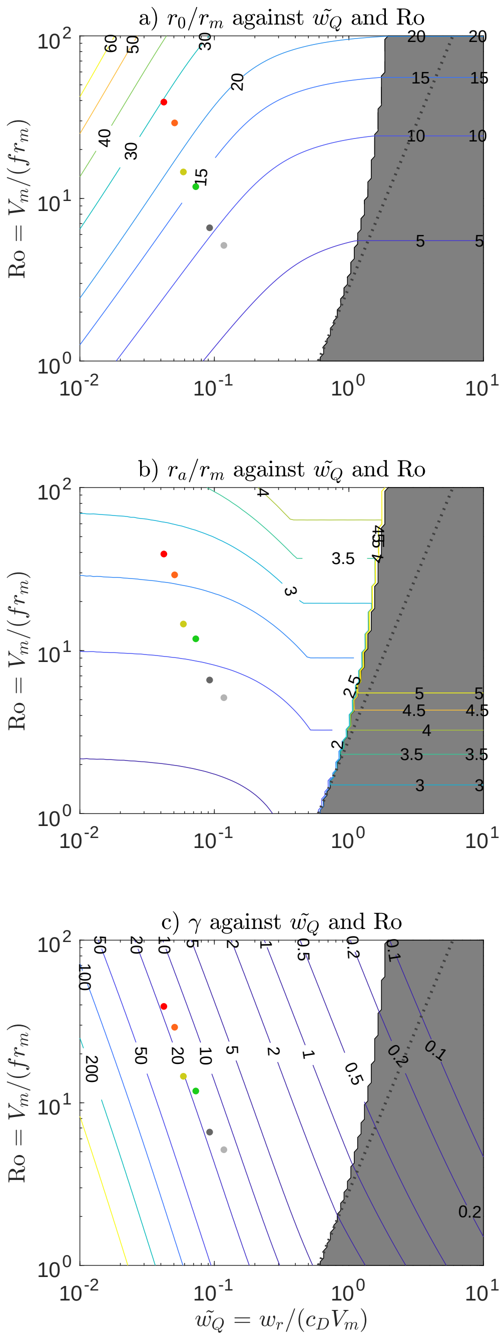

Figure 3. a) Normalized outer radius, r_0/r_m, for merged solutions as a function of nondimensional radiative-subsidence parameter $\tilde{w_Q}$ and inner core Rossby number Ro. Gray shading indicates the region of parameter space where the no outer wind solution is needed, and the black dotted line shows an approximate bound on this limit (Equation 16). Colored dots represent observed median storms from different intensity categories of Chavas et al. (2015); intensity increases from gray to red (see text for more details). b) Normalized merge radius r_a/r_m: inner solution applies for $r < r_a$ and outer solution for $r > r_a$. c) Outer wind nondimensional parameter γ.

Supporting Information for "An analytic model for Tropical Cyclone outer winds"

Timothy W. Cronin[1]

[1]Program in Atmospheres, Ocean, and Climate, MIT, Cambridge, Massachusetts, USA

Contents of this file

1. Text S1 to S5

2. Figure S1

Text S1: Fast calculation of multiple $G(r)$ profiles.

Matrix multiplication enables fast simultaneous calculation of $G(r)$ at many radial points and values of γ. The denominator y in $G(r)$ can be written as:

$$y = \sum_n \sum_l c_{n,l} \gamma^l [x^n/(n!)^2], \tag{1}$$

where the set of $c_{n,l}$ define a coefficient matrix C that depends on neither γ nor $x = 1 - r/r_0$. The coefficient of $[x^n/(n!)^2]$, or $(n!)^2 a_n = \sum_{l=0}^{\infty} c_{n,l}\gamma^l$, is a degree-$n$ polynomial in γ, defined by a linear, homogeneous, second-order recurrence relation with non-constant coefficients (Equation 10 in the main text, and note thereafter). I have found no closed-form solution for this recurrence, but an $N \times N$ coefficient matrix C needs only be computed once in order to make many calculations of G. For example, a single value of y can be written as a product of a row vector of powers of x, the coefficient matrix C, and a column vector of powers of γ, with an expression for the first four terms in y as follows:

$$y = \underbrace{\begin{bmatrix} x^0 & x^1 & \frac{x^2}{(2!)^2} & \frac{x^3}{(3!)^2} & \frac{x^4}{(4!)^2} \end{bmatrix}}_{X} \underbrace{\begin{bmatrix} 1 & 0 & 0 & 0 & 0 \\ 0 & 1 & 0 & 0 & 0 \\ 0 & 0 & 1 & 0 & 0 \\ 0 & 0 & -1 & 1 & 0 \\ 0 & 0 & -6 & -4 & 1 \end{bmatrix}}_{C} \underbrace{\begin{bmatrix} \gamma^0 \\ \gamma^1 \\ \gamma^2 \\ \gamma^3 \\ \gamma^4 \end{bmatrix}}_{\Gamma}. \tag{2}$$

To make many calculations at once, the row vector of powers of $x^n/(n!)^2$ is extended into a $K \times N$ (row $\times$ column) matrix X for K values of $x = 1 - r/r_0$, and the column vector of powers of γ is extended into a $N \times L$ matrix Γ for L values of γ. A $K \times L$ array of values of $y = XC\Gamma$ is thus given by matrix multiplication. The coefficients in $y'_{(x)}/\gamma$ can be written similarly, with a coefficient matrix C' obtained by deleting the first row and column of C, and multiplying the (new) n^{th} row by $n + 1$. The value of $G(r)$ is then calculated simultaneously for K points in radius and L values of γ using elementwise division of the matrices $y'_{(x)}/\gamma$ and y. Note that the factors $1/(n!)^2$ can be included in either powers of x or in the n^{th} row of C – they are written here in the matrix X, but numerical calculations (Cronin, 2023) include them in the matrix C for reasons of numerical precision ($(n!)^2$ becomes quite large).

Text S2: Approximations and convergence of $G(r)$.

I have not found any simplifications of $G(r)$ that are mathematically justified over the full range of r, but $G(r)$ can be approximated exactly near $r = r_0$ ($x << 1$) by a ratio of Bessel functions (dashed lines in Figure 2a). This approximation $G_b(r)$ is obtained by taking $1 - x \approx 1$ and $2 - x \approx 2$ in Equation 10 of the main text, which leads to an equation for an approximate solution y_b:

$$xy_{b(x)}{}'' + y_{b(x)}{}' - \gamma y_b = 0. \tag{3}$$

Relevant solutions of this equation are $y_b = I_0\left[2\sqrt{\gamma x}\right]$, where I_0 is the modified Bessel function of the first kind of order 0; leading to approximate solution $G_b(r)$:

$$G_b(r) = \frac{1}{\sqrt{\gamma x}} \frac{I_1\left[2\sqrt{\gamma x}\right]}{I_0\left[2\sqrt{\gamma x}\right]}. \tag{4}$$

This approximate solution also corresponds to the functional form of a simplified recurrence relation $a_n = \gamma a_{n-1}/n^2$, or (equivalently) setting all off-diagonal elements in the coefficient matrix C to zero. Some effort was devoted to using this Bessel function approximation as an initial guess at $G(r)$, and refining this guess with an analytically-determined correction function (which would take the form of a power series), but numerical evaluation of Equation 4 was found to be slower than simply evaluating the full solution $G = y'_{(x)}/(\gamma y)$ derived in the main text.

Empirically, I have found that the approximation:

$$G_e(r) = (1 + \gamma x)^{-1/2 - x/6} \tag{5}$$

works rather well (dotted lines in Figure 2a). Maximum relative errors for G_e are small when γ is small, but grow with increasing γ to $\sim 15\%$ for $\gamma = 100$ and $\sim 35\%$ for $\gamma = 1000$. The form $[1 + \gamma x]^{-1/2}$ was chosen to match the limiting value and slope of G at $r = r_0$, and the addition of the term $-x/6$ to the exponent was purely empirical; there is no theoretical basis for this choice.

Another approximation merits brief mention: Emanuel (2004) suggests that the dominant balance of terms in Equation 4 of the main text is such that both sides approximately equal zero, so that:

$$V(r) = \left(w_r f \frac{(r_0^2 - r^2)}{2c_D r} \right)^{1/2}. \tag{6}$$

This can be rewritten in terms of V_{AMC} and a relative wind speed factor G_{E04}, as:

$$V(r) = V_{AMC}(r) \underbrace{\left[\left(\frac{2}{\gamma} \frac{r/r_0}{1-(r/r_0)^2} \right)^{1/2} \right]}_{G_{\mathrm{E04}}(r)}. \tag{7}$$

This form appears to be a good approximation at intermediate radii when γ is large, but since the term in brackets approaches zero at $r = 0$ and blows up as $r \to r_0$, it fails at both large and small radii.

It is not obvious from the series solution (Equations 11 and 12 in main text) that the quotient $y'_{(x)}/(\gamma y)$ must be constrained to lie on $[0, 1]$. Calculations show rapid convergence for small γ, and slowest convergence for large γ (e.g., Figure 2b). The recurrence relation (Equation 11 of the main text) is consistent with this result: it indicates that coefficients in the series will increase in magnitude roughly until $n > \sqrt{\gamma}$, and decay roughly as 2^{-n} at $n >> \sqrt{\gamma}$, suggesting that the required number of terms for convergence should scale with $\sqrt{\gamma}$. Since the range of values of γ for realistic cyclones is relatively constrained, good accuracy can be obtained if a number of terms several times as large as the square root of the greatest value of γ experienced is used (Figure 2b or other similar calculations can guide such decisions).

Text S3: Situations with no outer-wind component

A first-order approximation to $G(r)$ can be used to derive a condition on the values of $\tilde{w_Q}$ and Ro for which there is no outer wind component to the merged profile. The merged profile will consist of an inner-wind only profile if the inner and outer wind profiles do not intersect on $0 < r < r_0$ when r_0 is set equal to $r_i = r_m(4V_x/(fr_x) + 1)^{1/2}$, the radius where the inner wind profile goes to zero. For the math in this section, it is sufficiently accurate to assume $V_x \approx V_m$ and $r_x \approx r_m$, so that $r_i/r_m = (4\mathrm{Ro} + 1)^{1/2}$.

I begin by rewriting Equation 13 of the main text as:

$$V_{\mathrm{in}} = f\frac{r_i^2 - r^2}{2r} \times \frac{(r/r_m)^2}{1 + (r/r_m)^2}, \tag{8}$$

which is akin to Equation 8 of the main text, in that it expresses the winds as an angular-momentum-conserving value, multiplied by a function of radius that lies between 0 and 1 and increases monotonically with increasing r. Equating the inner and outer wind profiles when $r_0 = r_i$ to solve for radii r^* where the two profiles intersect requires that $G(r^*) = (r^*/r_m)^2/(1 + (r^*/r_m)^2)$ for the outer wind profile. There will thus be no physical merge radius possible if the outer wind profile has $G(r) > (r/r_m)^2/(1+(r/r_m)^2)$ for all $0 < r < r_i$. Since this limit only appears to occur (see the gray shaded area in Figure 3) when $\tilde{w_Q}$ is large and γ is small, I use a first-order approximation of $G(r) \approx 1 - \gamma(1 - r/r_0)/2$ in γ. Rearranging the equality $G(r^*) = (r^*/r_m)^2/(1+(r^*/r_m)^2)$ with this small-γ approximation for $G(r)$ gives:

$$\frac{2}{\gamma} = (1 + (r^*/r_m)^2)(1 - r^*/r_0), \tag{9}$$

which will lack a solution if the maximum value of the right-hand side on $0 < r^* < r_0$ is less than the value of the left-hand side. In the limit that Ro is reasonably large, $r_0 = r_i \approx 2r_m\mathrm{Ro}^{1/2}$, and the value of the right-hand side maximizes at approximately $16\mathrm{Ro}/27$ for $r^* \approx 2r_i/3 >> r_m$. In this limit, the left-hand side can also be approximated as $2/\gamma \approx 2w_r/(2r_m\mathrm{Ro}^{1/2}fc_D) = Ro^{1/2}\tilde{w_Q}$. Equating these expressions indicates that the left-hand side will be larger than the maximum value of the right for all $0 < r^* < r_0$ if $\tilde{w_Q}$

exceeds some critical value $\tilde{w_Q}^*$, where:

$$\tilde{w_Q}^* = \frac{16\mathrm{Ro}^{1/2}}{27}. \tag{10}$$

Thus, if $\tilde{w_Q} > \tilde{w_Q}^*$, this argument indicates no outer-wind component; this region lies to the right of the dark gray dotted line in Figure 3.

Text S4: Benchmarking for merged wind calculations

I include MATLAB code that performs fast calculations of the merged $V(r)$ profiles (Cronin, 2023). The code is faster than previous approaches for two main reasons. First, a lookup table approach is used to store r_0/r_m, r_a/r_m (and thus also γ) as functions of $\tilde{w_Q}$ and Ro – this is feasible because analytic solutions to the outer wind profile allow storing entire profiles across a broad range of parameter space with only a few saved variables. the code interpolates from generic input values of $0.01 < \tilde{w_Q} < 10$ and $1 < \mathrm{Ro} < 100$ to obtain r_0/r_m and r_a/r_m, which determine γ and the radial domain of each wind model. Second, the code is fast because it is vectorized: the matrix approach above (Text S1) allows calculation of many values of $G(r)$ at once. These two improvements increase the calculation speed for wind profiles by a factor of ~ 50 relative to the code of Chavas (2022) (Figure S1a). The codes are compared by selecting 100 random points from parameter space with $17 < V_m < 77$ m s^{-1}, $15 < r_m < 115$ km, $5 \times 10^{-5} < f < 1.25 \times 10^{-4}$, and $0.001 < w_r < 0.005$ m s^{-1}, and a constant value of $c_D = 0.0015$. The lookup/matrix method described above gets faster in a relative sense for more profiles computed at once, so long as there is sufficient memory.

In terms of accuracy, differences between the two codes in azimuthal winds are typically on the order of 0.1 m s^{-1} (Figure S1b). Further testing suggests this small difference in winds between the two codes arises from a combination of factors, including the precision of wind merger of the two profiles in both codes, the method of tweaking of V_x and r_x in the inner wind profile to ensure that $\max(V)$ occurs at $r = r_m$ in both codes, the table lookup interpolation and power series truncation errors in my method, and numerical integration errors in the approach of Chavas (2022). My code seems to be converged more closely to a "true" solution than calculations with default parameters of Chavas (2022), and the approach here can also use decreased grid spacing without degrading accuracy. Overall, the code presented here (Cronin, 2023) may be useful for risk modeling or probabilistic forecasting applications where it is desirable to simulate the effects of a very large number of realizations of wind profiles.

Text S5: Overturning streamfunction of the inner wind model

The overturning circulation and integrated vertical mass transport of a Tropical cyclone is given (under the assumption of a balance between radial advection of angular momentum and frictional torque) by rearranging Equation 1 of the main text:

$$\psi = \frac{c_D r^2 V^2}{dM/dr}, \tag{11}$$

where the overturning streamfunction ψ thus has units of m^3 s^{-1} (mass and volume transports are used interchangeably here following Emanuel, 2004, which is not completely accurate but suffices for the purposes here). Because V and dV/dr are continuous at the merge radius r_a, merged wind profiles are also continuous in dM/dr and ψ. Although not discussed as rationale by Chavas, Lin, and Emanuel (2015), continuity of the streamfunction is a critical reason to enforce continuity of dV/dr at the merge point. The inner wind profile of Emanuel and Rotunno (2011), with $c_k/c_D = 1$, has wind profile given by

Equation 13 of the main text, which can be rewritten for the sake of the scaling argument here using the approximate equalities $V_x \approx V_m$, $r_x \approx r_m$, and $V_x/(fr_x) \approx \mathrm{Ro}$. The inner wind model thus has streamfunction:

$$\psi_{\mathrm{in}} = \frac{c_D V_m r_m^2}{16\mathrm{Ro}^2\left(1+\frac{1}{2\mathrm{Ro}}\right)}\left(\frac{r}{r_m}\right)^3\left[(4\mathrm{Ro}+1)-\left(\frac{r}{r_m}\right)^2\right]^2. \tag{12}$$

This inner streamfunction can be shown to maximize at $r/r_m = \sqrt{\frac{3}{7}(4\mathrm{Ro}+1)}$, which is typically a considerably greater radius than $r_a/r_m \sim 3$ shown by Figure 3 (this result is also implied by the shape of the inner streamfunction in Figure 1). The positive value of $d\psi/dr$ at the merge point for the parameter space occupied by real-world storms indicates that r_a is generally small enough that inner circulation still has strong ascent there. This is consistent with the statement by Chavas et al. (2015) that the merged profiles represent an "ascending inner region" patched to a "descending outer region." This point should not be seen as a foregone conclusion because the inner wind profile itself contains both an inner ascending region where $r/r_m < \sqrt{\frac{3}{7}(4\mathrm{Ro}+1)}$, and an outer descending region where $r/r_m > \sqrt{\frac{3}{7}(4\mathrm{Ro}+1)}$.

Evaluating $\psi_{\mathrm{in}}(r_a)$ gives the net upward mass transport by the storm. In the limits – reasonable for real-world storms – that Ro>> 1 and $r_a/r_m << \sqrt{4Ro+1}$, this mass transport is given by:

$$\psi_{\mathrm{in}}(r_a) \approx c_D V_m r_m^2 \left(\frac{r_a}{r_m}\right)^3. \tag{13}$$

This result is used further in the main text to explain the interdependence of V_m, r_m, and r_0 for merged profiles, and generally indicates strong sensitivity of the upward mass transport of a cyclone to the radius of the ascending region r_a.

References

Chavas, D. R. (2022, Jun). *Code for tropical cyclone wind profile model of Chavas et al (2015, JAS).* Retrieved from `https://purr.purdue.edu/publications/4066/1` doi: 10.4231/CZ4P-D448

Chavas, D. R., Lin, N., & Emanuel, K. (2015). A model for the complete radial structure of the tropical cyclone wind field. Part I: Comparison with observed structure. *Journal of the Atmospheric Sciences*, *72*(9), 3647–3662.

Cronin, T. W. (2023, Mar). *Code for "An analytic model for Tropical cyclone outer winds".* Retrieved from `https://doi.org/10.5281/zenodo.7783251` doi: 10.5281/zenodo.7783251

Emanuel, K. (2004). Tropical cyclone energetics and structure. *Atmospheric turbulence and mesoscale meteorology*(8), 165–191.

Emanuel, K., & Rotunno, R. (2011, 2012/01/04). Self-stratification of tropical cyclone outflow. Part I: Implications for storm structure. *Journal of the Atmospheric Sciences*, *68*(10), 2236–2249.

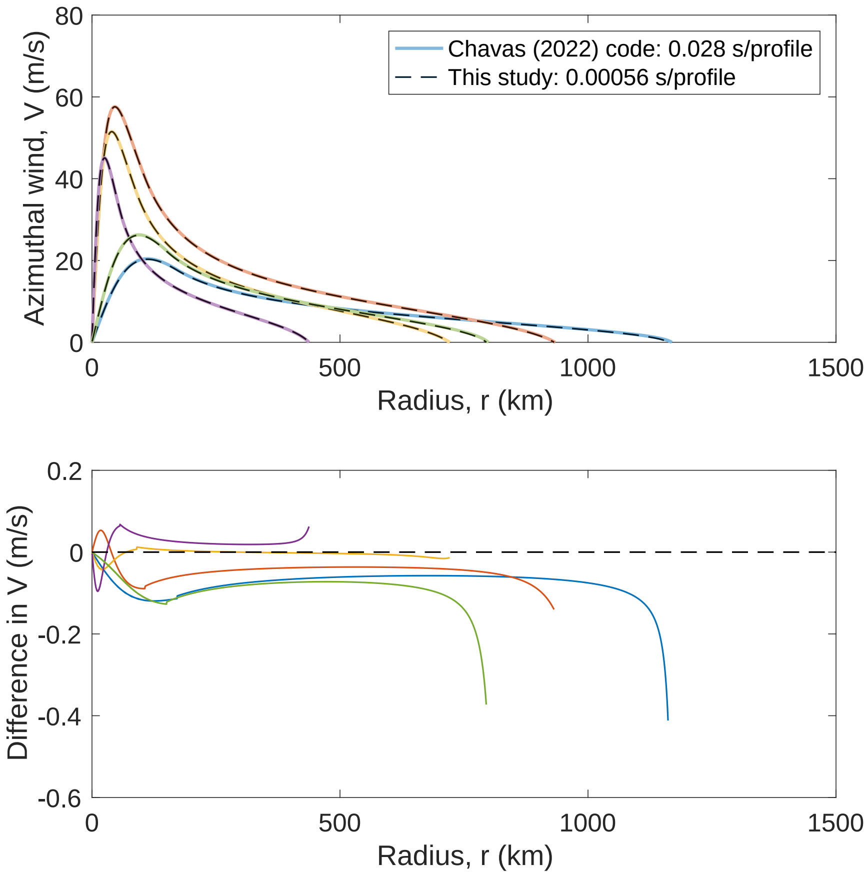

Figure S1. a) A set of five random wind profiles from a benchmark calculation on 100 random parameter values comparing the code from this study to the previous numerical method of Chavas (2022). b) Wind difference as a function of radius relative to the previous numerical method of Chavas (2022).